Eddy Current Losses Calculation in Rotor Back Iron and Magnet for Concentrated Winding Permanent Magnet Generator

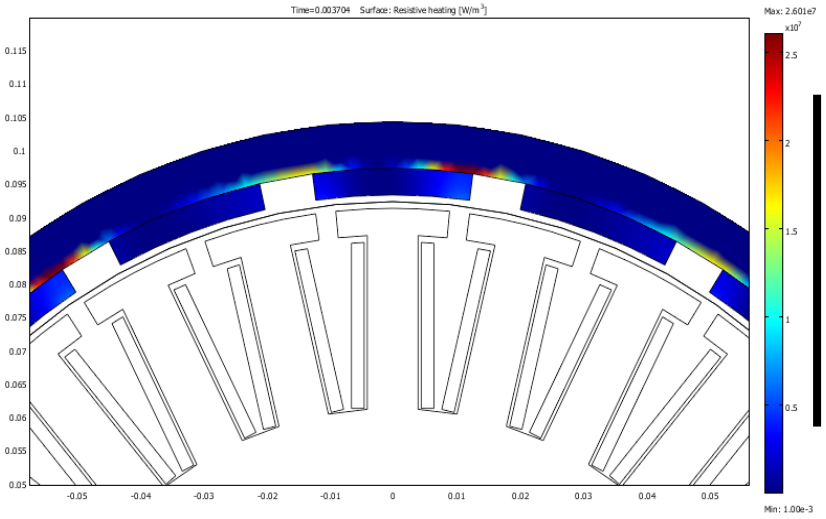

Author:
Muhammad Firmansyah

Student Number:
1389246

Date:
27 August 2009

Thesis Committee

Prof. J.A Ferreira
Dr. Henk Polinder
Dr. Domenico Lehaye
Ir. Anoop K. Jassal

EEC

Electrical Energy Conversion

TU Delft

Delft University of Technology

ABSTRACT

Concentrated winding is proposed to replace distributed winding due the advantages in manufacturing process. It is easily wound by machine in the former and the impregmentation process can be carried out separately for each individual coil. These advantages can lead to automation process in winding processes, reduce time and cost for generator manufacturing.

One of the problems in concentrated winding generator is eddy current losses, due to the fact that air gap flux in concentrated winding contains much more harmonics compared to the distributed winding. These losses should be kept within the acceptable level of heat removing capability of generator; otherwise higher temperature of magnet could influence the remanence flux of permanent magnet.

In this thesis two methods of eddy current losses calculation, analytical and finite element (FE) are presented. Finite Element Method has some advantages due its capability to handle the geometric problem and non linear material which is difficult to incorporate in analytical calculation.

ACKNOWLEDMENTS

Thanks to my company PT PLN (persero) for providing the facilities to study in TU Delft, many thanks to my thesis committee (Dr.H.Polinder,Dr.Domenico Lehaye, Ir.Anoop.K.Jassal and Prof.J.A fereira) for spent a lot of time for discussion and guidance.

To my Wife, my children, my parents and my family, thanks for your patient, love and pray.

Thanks to 'Syaikh" Dedy Wicaksono to repair my final report, to all off PLN'ers (Edy, elpis, Buyung, Handy, Didik, Himmel, Jarot, Endah,Dwi,Lucky,Asyrof,Lambas,Chris) thanks to all of your help during this two years, to all of PPI Delft'ers (Yugi,Dira,Baqir,Angga,etc) thanks to warm of friendship. Many thanks to all of KM Delft family (Azwar, Miftah,Agung,Khatami,Zaiyan,Rik-rik,Egon.Heri, Ucup.etc) to warm of brotherhood. Thanks to the students of EEC Group (Jeremy, Lu Ni, Albert. etc) for free coffee and a lot of joke in our room. "May God bless you all".

TABLE OF CONTENT

LIST OF FIGURES

LIST OF TABLES

Chapter 1

INTRODUCTION

This chapter will present the background of the topic choice, problem definition and the layout of this thesis

1.1 Background

Energy demand in the future will increase rapidly due to the increase of population, and industrialization as well as increase in households' energy consumption in developing countries. These factors will affect the energy prices and depletion of conventional fuels like coal, gas and oil. The increase of energy consumption will add more to the environmental problems due to the production of green house gases during the conversion or consumption of energy.

Based on the Kyoto protocol, the European Union is committed to decrease the green house gas concentration in air by 20% by the year 2020 and to 50% in 2050 compared to its level in 1990. Four steps to achieve these goals are presented in the green paper on energy policy in Europe [1]

1. Increase the energy efficiency
2. Increase the proportion of renewable energy in energy mix
3. Apply alternative fuel for transportation sector
4. Liberalization of interconnection energy system

Figure.1 shows new electric power generation installed between the year 2000 and 2007. Wind energy takes a part of 46.8 GW. This trend predicted will continue and get stronger due to the success of wind turbine technology.

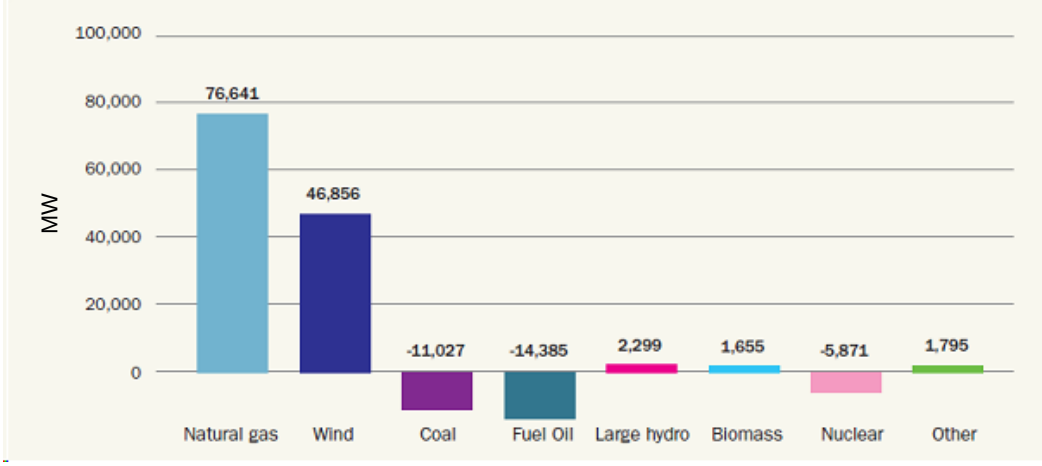

Figure 1.1 Net installed capacity by fuel in European Union 2000-2007

Source: http://www.ewea.org/fileadmin/ewea_documents/documents/statistics/energy_mix.pdf

European Wind Energy Association (EWEA) projects the reference scenario trends of accumulated wind turbine capacity installed to increase by 80 GW in 2010, 180 GW in 2020 and 300 GW by 2030 [2]. A number of annual installations based on this scenario are shown in figure 1.2. With an average of 10 GW annually installed capacity. If we assume an average capacity of one unit wind turbine to be 2.5 MW, then at least 4000 unit of wind turbine are needed every year in European market.

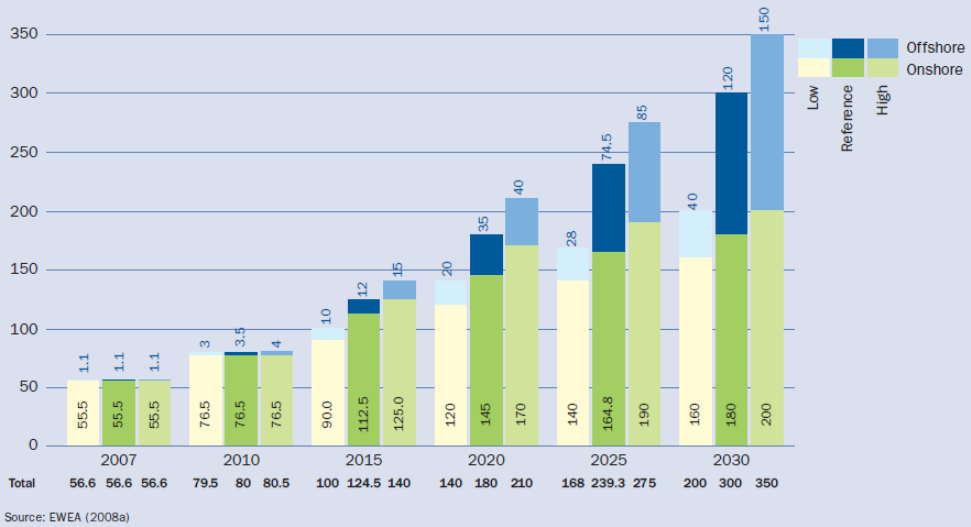

Figure 1.2 Projection of wind turbine installation in Europe

Source: http://www.ewea.org/fileadmin/ewea_documents/documents/publications/WETF/1565_ExSum_ENG.pdf

The growth of wind energy demand will be followed by the increasing number of wind turbine generator installed. To full-fill the demand, generator manufacturing process should take less time and cost. The automation process in many cases is the best way to get lower price and faster time in manufacturing stage.

The obstacle in automation process of wind turbine is the fact that not all processes of wind turbine generator manufacture can be carry out automatically, for example in winding process with distributed winding type., Figure 1.3 shows the winding process of generator that should be carried out manually which takes time and cost.

As an Alternative solution to this problem, concentrated winding has been proposed to replace distributed winding. Concentrated winding can be easily wound by machine in the former; the former size is replicated from the size of the tooth. Another advantage of concentrated winding is in impregmentation process, the impregmentation can be carried out separately for each individual coil, while in distributed winding it should be carried out together, and thus it would need a very big tank and oven due to the large size of the machine.

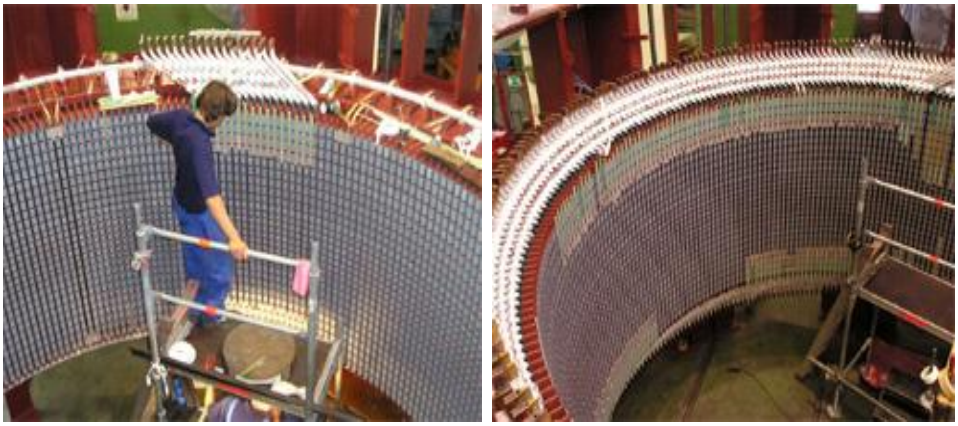

Figure 1.3 Stator Winding Process of Generator

Source: http://www.stork.com/eCache/DEF/13/018.html

1.2 Problem definition

Concentrated winding in permanent magnet generator (PMG) has been introduced in [4,5] as an alternative for distributed winding. This winding type has several advantages:

- Easy to manufacture automatically
- Lower winding losses
- With a number of design constrains, the generator can operate in fault tolerance condition.

However, one of the problems in concentrated winding generator is eddy current losses, due to the fact that air gap flux in concentrated winding contains much more harmonics compared to the distributed winding. High frequency air gap harmonic will induce much higher eddy current losses.

The other source of harmonics in air gap flux is non-sinusoidal current in the winding due to the loading of the generator by power electronic converter in direct drive wind turbine topology. Figure 1.4 (a) illustrates air gap mmf from concentrated winding and figure 1.4 (b) shows the Fourier series from air gap mmf.

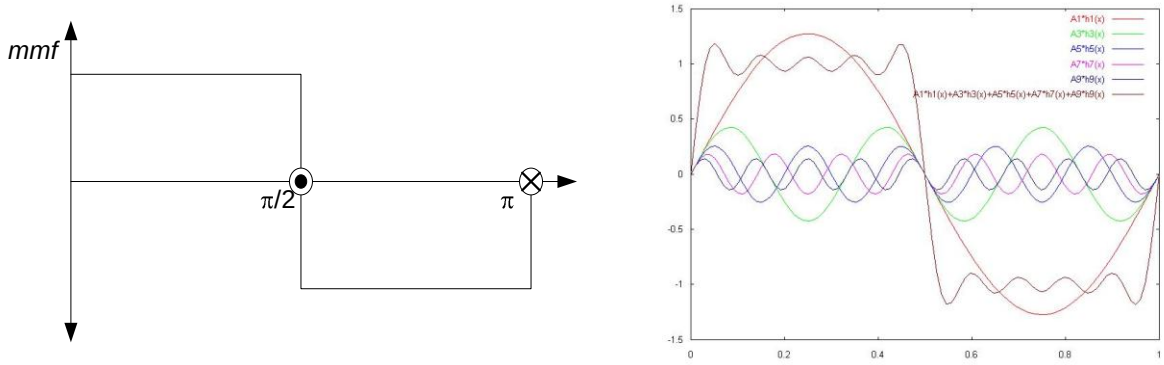

(a) (b)

Figure 1.4 Concentrated winding (a) Air gap MMF (b) Air gap MMF Fourier series

The level of eddy current will determine the losses in permanent magnet and rotor core (back iron). This loss should be kept within the acceptable level of heat removing capability of generator; otherwise higher temperature of magnet could influence the remanence flux of permanent magnet.

References [12-15] show the analytical solution to compute Eddy current losses in Back Iron and Permanent Magnet. In order to get a better calculation for eddy current losses in back iron and magnet during the design process, this thesis will deal with the calculation of eddy current in back iron and permanent magnet using Finite Element Method.

Finite Element Method has some advantages due its capability to handle the complex geometric problem and non linear material which is difficult to incorporate in analytical calculation [6-10].

1.3 Thesis lay out

The content of this thesis will consist of Introduction in chapter I, to give the overview of the back ground and problem definition. Chapter II reviews the Electromagnetic Theory relevant for the modeling. Chapter III introduces the Finite Element Method. Chapter IV describes the three model of machine and analytical calculation for eddy current losses in back iron and magnet.

Chapter V contains the FEM losses computation result. Chapter VI presents comparison between Analytical and FEM results. Chapter VII contains the conclusion and some suggestions for future work.

Chapter 2

OVERVIEW OF ELECTROMAGNETIC THEORY

This chapter will present the overview of electromagnetic theory starting with Maxwell equation, boundary and non-linear material problem, force and torque calculation and eddy current losses in back iron and permanent magnet

2.1 Maxwell's equations

Time-varying electromagnetic field represents two concepts; magnetic field produced by a changing electric field and electric field produced by changing magnetic field. Here we rewrite the fundamental electromagnetic quantities with the unit [6]: magnetic field strength **H** [Ampere.m^{-1}] , magnetic flux density **B** [Tesla], electric field strength **E** [Volt.m^{-1}], electric flux density **D**[Coulomb.m^{-2}], current density **J**[Ampere.m^{-2}], electric charge density ρ[Coulumb.m^{-3}]. **,** and differential form for time-varying magnetic field equation

$$\nabla \times \boldsymbol{H} = \boldsymbol{J} + \frac{\partial \boldsymbol{D}}{\partial t} \tag{2.1}$$

$$\nabla \times \boldsymbol{E} = -\frac{\partial \boldsymbol{B}}{\partial t} \tag{2.2}$$

$$\nabla . \boldsymbol{B} = 0 \tag{2.3}$$

$$\nabla . \boldsymbol{D} = \rho \tag{2.4}$$

Equation (2.1) known as Ampere-Maxwell law, equation (2.2) as Faraday law, equation (2.3) as Gauss-Faraday law, (2.4) Gauss law, the **J** and **ρ** can be considered as source which determine the **H, B, E** and **D** also correlated with the continuity equation

$$\nabla . \boldsymbol{J} = -\frac{\partial \rho}{\partial t} \tag{2.5}$$

In linear isotropic material, the constitutive equations which describe macroscopic properties of the medium are as follow

$$\boldsymbol{J} = \sigma \boldsymbol{E} \tag{2.6}$$

$$\boldsymbol{B} = \mu \boldsymbol{H} \tag{2.7}$$

$$\boldsymbol{D} = \varepsilon \boldsymbol{E} \tag{2.8}$$

Where σ [$ohm^{-1}.m^{-1}$] is electric conductivity, μ [$Henry.m^{-1}$] magnetic permeability and ε [$Farad.m^{-1}$] dielectric constant or permittivity.

2.2 Magnetic vector potential

Since the field vector B satisfied a zero divergence condition (2.3), it can be expressed in term of vector magnetic potential **A** as follows

$$\boldsymbol{B} = \boldsymbol{\nabla} \times \boldsymbol{A} \tag{2.9}$$

From equation (2.9) and (2.2)

$$\boldsymbol{\nabla} \times \left(\boldsymbol{E} + \frac{\partial \boldsymbol{A}}{\partial t}\right) = 0 \tag{2.10}$$

Hence, by integration, one obtains

$$\boldsymbol{E} = -\boldsymbol{\nabla} \boldsymbol{V} - \frac{\partial \boldsymbol{A}}{\partial t} \tag{2.10}$$

V is scalar potential. Neither **A** nor ***V*** are completely defined since the gradient of an arbitrary scalar function can be added to A and time derivatives of the same function can be subtracted from **V** without affecting physical quantities **E** and **B**, this transformation is called the gauge transformation.

In the magneto-static case, where there is no current present, equation 2.1 reduce to $\boldsymbol{\nabla} \times \boldsymbol{H} = 0$, and we define magnetic scalar potential by following relation

$$\boldsymbol{H} = -\boldsymbol{\nabla} \boldsymbol{V}_m \tag{2.11}$$

2.3 Boundary condition

Between two different dielectric materials, we also need to specify conditions at the material interface. We can express mathematically as follow

$$\boldsymbol{n}_2 \times (\boldsymbol{E}_1 - \boldsymbol{E}_2) = 0 \tag{2.11}$$

$$\boldsymbol{n}_2 . (\boldsymbol{D}_1 - \boldsymbol{D}_2) = \rho_s \tag{2.12}$$

$$\boldsymbol{n}_2 \times (\boldsymbol{H}_1 - \boldsymbol{H}_2) = \boldsymbol{J}_s \tag{2.13}$$

$$\boldsymbol{n}_2 . (\boldsymbol{B}_1 - \boldsymbol{B}_2) = 0 \tag{2.14}$$

And for current density condition on interface

$$\boldsymbol{n}_2 . (\boldsymbol{J}_1 - \boldsymbol{J}_2) = \frac{\partial \rho_s}{\partial t} \tag{2.15}$$

The boundary between dielectric material with conductor will have condition $\mathbf{D_1}$ = 0 and $\mathbf{E_1}$=0, and for time varying $\mathbf{B_1}$ = 0 and $\mathbf{H_1}$=0, and the set of boundary condition become

$$-\boldsymbol{n}_2 \times (\boldsymbol{E}_2) = 0 \tag{2.16}$$

$$-\boldsymbol{n}_2 . (\boldsymbol{D}_2) = \rho_s \tag{2.17}$$

$$-\boldsymbol{n}_2 \times (\boldsymbol{H}_2) = J_s \tag{2.18}$$

$$-\boldsymbol{n}_2 . (\boldsymbol{B}_2) = 0 \tag{2.19}$$

2.4 Two dimensional time varying field

In time-varying magnetic field, with frequency less than 10^4 Hz, we can neglect the change of electric flux density in time [6]($\delta\mathbf{D}/\delta t = 0$) (this condition is called as the quasi static field), let we consider equation 2.6 and substitute it into equation 2.1

$$\nabla \times \boldsymbol{H} = \sigma \boldsymbol{E} \tag{2.20}$$

From equations 2.9 and 2.7

$$\nabla \times \left(\frac{1}{\mu}\nabla \times \mathbf{A}\right) = \sigma \boldsymbol{E} \tag{2.21}$$

From ohm law

$$\nabla \times \left(\frac{1}{\mu}\nabla \times \mathbf{A}\right) = \boldsymbol{J} \tag{2.22}$$

From equations 2.10 and 2.6

$$\sigma \boldsymbol{E} = -\sigma \nabla \boldsymbol{V} - \sigma \frac{\partial \boldsymbol{A}}{\partial t} \tag{2.23}$$

The component of J can be separated into external current ($\sigma \nabla \boldsymbol{V}$) and induced current($\sigma \frac{\partial \boldsymbol{A}}{\partial t}$), thus from equations 2.21 and 2.23 we can get the following expressions

$$\nabla \times \left(\frac{1}{\mu}\nabla \times \mathbf{A}\right) = -\sigma \nabla \boldsymbol{V} - \sigma \frac{\partial \boldsymbol{A}}{\partial t} \tag{2.25}$$

Modeling the machine with finite element can be carried out in two or three dimensional magnetic field. Considering the time consumption for computation and the extracted data that we want to analyze for computing eddy current loses in back iron and permanent magnet, we can choose two dimensional models with some assumption taken into account for simplification.

In two dimensional magnetic fields, we assume that the current flows only in the z direction hence $\mathbf{A}_z$ only exist, and this quantity does not change in the z direction. Let us take equations 2.9 and 2.1 in quasi static condition they become,

$$\boldsymbol{B}_x = \frac{\partial \boldsymbol{A}_z}{\partial y}, \boldsymbol{B}_y = -\frac{\partial \boldsymbol{A}_z}{\partial x} \tag{2.26}$$

From constitutive relation in equation 2.7, equation 2.23, substitute equation 2.26 into equation 2.9, since J only in z direction (J_z)

$$\sigma \frac{\partial \boldsymbol{A}_z}{\partial t} + \frac{\partial}{\partial x}\left(\frac{1}{\mu_0 \mu_r}\frac{\partial \boldsymbol{A}_z}{\partial x}\right) + \frac{\partial}{\partial y}\left(\frac{1}{\mu_0 \mu_r}\frac{\partial \boldsymbol{A}_z}{\partial y}\right) = -\boldsymbol{J}_z \tag{2.27}$$

2.5 Permanent magnet

There are two types of permanent magnet characters: type 1 is metallic alloy material such as alnico or alcomax series, and type 2 is material which practically has linear characteristic (see figure 2.1). This type's representatives are the modern rare-earth materials such as samarium cobalt or neodymium iron boron. Two important features from permanent magnet are flux remanence (B_r) and coercive force (H_c). A magnet type 1 characteristic is shown in figure 2.1,

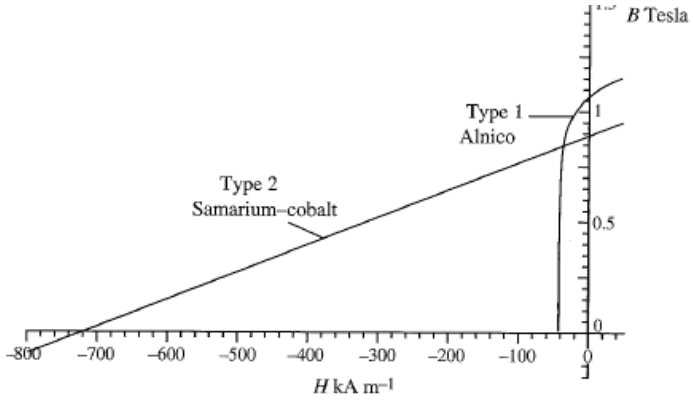

Figure 2.1 Typical permanent magnet characteristic, source [7]

The two types of characteristics lead to different performance when magnets are exposed to demagnetization, either by the effect of demagnetizing current or air gap. Consider a magnet type-1 with characteristic shown in figure 2.2. The magnet operating in point A, with flux density B_1 and magnetizing force H_1, The line OA is the load line, instead of the reluctance of the magnetic circuit.

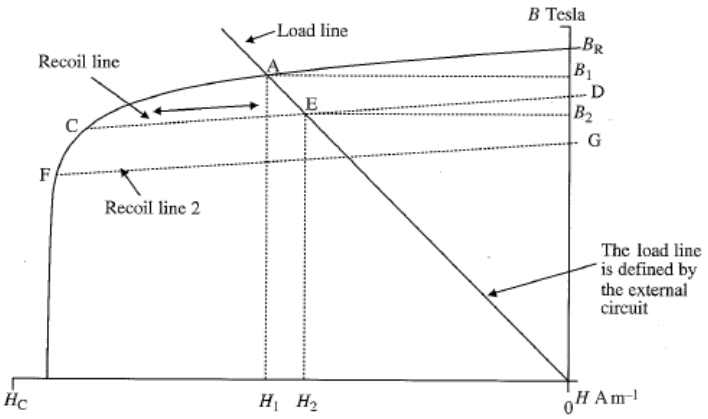

Figure 2.2 Permanent magnet dynamics, source [7]

If the demagnetization flux forces magnet move to point C, after removal of the flux, the magnet will work on recoil line CD which crosses the load line at Point E having at that situation the flux density $\mathbf{B}_2$ and the magnetizing force $\mathbf{H}_2$. The magnet characteristic can be described in two principal ways

$$\boldsymbol{B} = \boldsymbol{B}_r + \mu_o \mu_a H \text{ where } \mu_a = \frac{\boldsymbol{B}_r - \boldsymbol{B}}{\mu_o |\boldsymbol{H}|} \tag{2.26}$$

$$\boldsymbol{B} = \mu_o \mu_r (\boldsymbol{H} - \boldsymbol{H}_c) \text{ Where } \mu_r = \frac{\boldsymbol{B}}{\mu_o (\boldsymbol{H} - \boldsymbol{H}_c)} \tag{2.27}$$

Formulation for permanent magnet can be done in two ways: vector potential formulation and scalar potential formulation, using equation (2.27) and (2.9) and the fact that there are no current sources in magnet

$$\boldsymbol{\nabla} \times \left(\frac{\boldsymbol{B}}{\mu_o \mu_r}\right) = \boldsymbol{\nabla} \times \boldsymbol{\nabla} \times \left(\frac{\boldsymbol{A}}{\mu_o \mu_r}\right) \tag{2.28}$$

$$\nabla \times \nabla \times \left(\frac{A}{\mu_0 \mu_r}\right) + \nabla \times \boldsymbol{H_c} = 0 \qquad (2.29)$$

From equation 2.22, part $\nabla \times \nabla \times \left(\frac{A}{\mu_0 \mu_r}\right)$ is similar to current density **J**, so the $+\nabla \times \boldsymbol{H_c}$ term can be regarded as equivalent to the current density $\mathbf{J_m}$. $\mathbf{J_m}$ assumed constant within element., and the equivalent current (I_s) over the surface area S can then be formulated:

$$\int_S \boldsymbol{J_m} d_S = \boldsymbol{I_m} = \oint \boldsymbol{H_c} dl \qquad (2.30)$$

Equations (2.28)-(2-30) represent permanent magnet in vector potential form. To represent permanent magnet on scalar potential form, let us illustrate a simple ring magnet on figure 2.3(a), where we assume the change of l_m with radius is negligible, no leakage, area of air gap = area of magnet, $B_g = B_m = \mu_0 H_g$., by taking magnetic circuit and applying ampere law, we get following expression :

$$\boldsymbol{H_m} = -\boldsymbol{H_g} \frac{l_g}{l_m} \qquad (2.31)$$

Equation (2.31) is shown as point in the load line in figure 2.3(b)

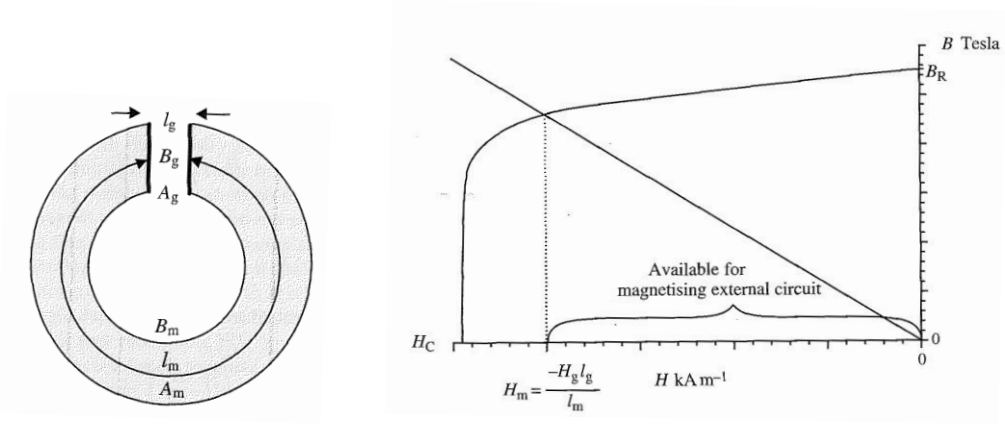

(a) (b)

Figure 2.3 (a) Ring magnet with air gap (b) Load line, source [7]

thus (H_C-H_m) Am^{-1} can be regarded as consumed in the magnet and H_m Am^{-1} as available to magnetize gap. The logical model for the scalar magnetic potential can be a setup having a number of shells with prescribed variation of potential dependent on the coercive force and the magnet length, linked with each shells (see figure 2.4)

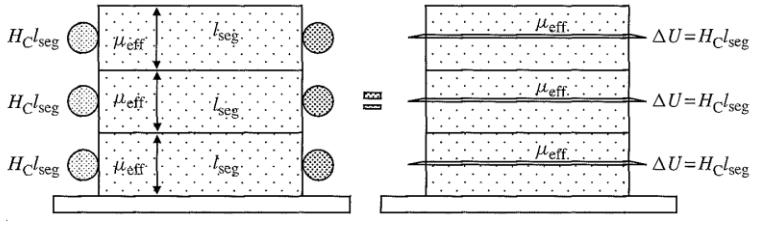

Figure 2.4 Shell representation of permanent magnet, source [7]

2.6 Non linear material

Reference [17] classifies the material properties into four groups:

1. Inhomogeneous material: is a medium where the constitutive parameters vary in the space coordinates. As a result field properties reign at different parts of material geometries
2. Anisotropic material: is a medium where the field relation at any point is diverse for different direction of propagation.
3. Nonlinear material: is a material where the permittivity or permeability vary with the intensity of electromagnetic field. This also includes hysteresis effect where the physical properties of material are influenced by the field strength and the field distribution.
4. Dispersive material: is a medium where the change in velocity of wave with wavelength is expressed by frequency dependence in constitutive laws.

Soft magnetic material is commonly used in generator as the material for stator and rotor; there are two basic types of soft magnetic material:

- Ferromagnetic material: based on iron and nickel, which are applicable lower frequencies less than 2 kHz.
- Ferrimagnetic materials, which are based on ceramic oxides of metals, and applicable to frequencies from a few kilohertz to well over 80 MHz

Correlation between B and H does not follow the constitutive relation in equation (2.7) but follow the characteristic of B-H Curve of the material

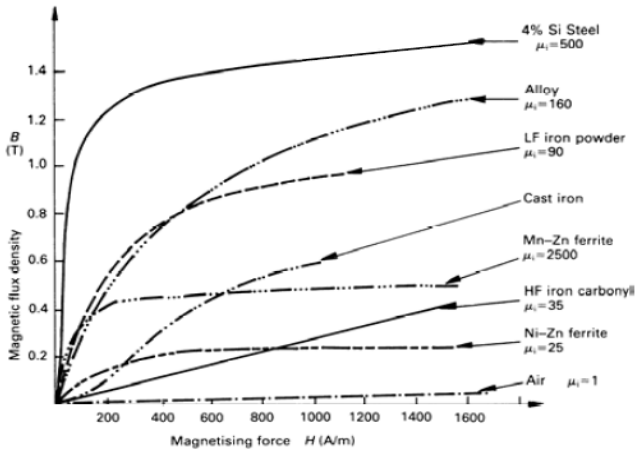

Figure 2.5 B-H Curve for various soft magnetic material [ ]

The relationship between B and H in ferromagnetic material expressed by

$$B = f(|H|) \tag{2.32}$$

There are three methods to solve equation (2.32)

2.6.1 Cyclic adjustment of permeability

This process is straightforward and intuitive, and used widely in early finite element works. However, the rate of convergence is uncertain, depending on the value of the error being set.

Flow chart of the processes are shown in figure 3.2, starts by assuming a value of permeability, solving the equation and computing the flux density and correcting the permeability so that it would be consistent with the computed value of current density. The equations are being solved again and new flux density is found, permeability is corrected, and the process continues until the result is established.

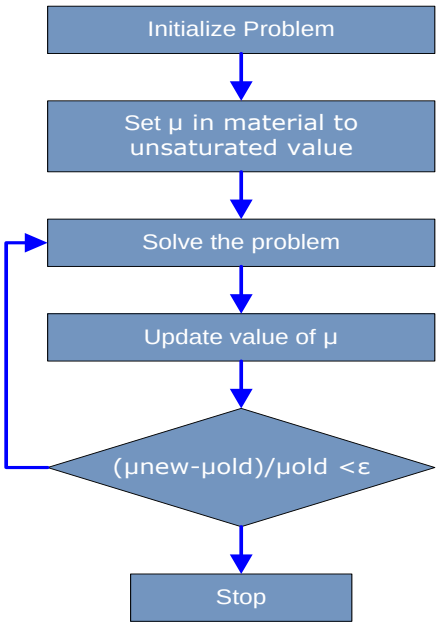

Figure 2.6 Cyclic adjustment of permeability

2.6.2 Newton-Rhapson iteration

The basic idea is to use the derivative of the function with respect to the quantity to be determined to steer the process towards a solution, In vector magnetic potential problem, the matrix will form : {S} {A} = {J}, where {S} = is a square reluctivity matrix, {A} is a column matrix, and {J} is column matrix of current. And the steps are:

- Make initial estimate of A
- Calculate initial error
- Derive corrections to initial value of A
- Obtain improved estimate of A
- Repeat the procedure until acceptable small correction is obtained

2.6.3 Analytical calculation of permeability

This method is presented in reference [18] , the aim of this method is to reduce the computational time by avoiding numerical calculation for permeability such as implemented by two

methods before. B-H curve of material is formed by measurement data and potentially to make convergence in FEM calculation flat stagnation. Magnetic material law is considered as follows

$$\boldsymbol{H}(\boldsymbol{B}) = \nu\boldsymbol{B} = \nu_0 \nu_r(\boldsymbol{B})\boldsymbol{B} \Leftrightarrow \nu(\boldsymbol{B}) = \frac{d\boldsymbol{H}}{d\boldsymbol{B}}(\boldsymbol{B}) \tag{2.33}$$

Where ν_0 and ν_r are the reluctivity of vacuum and the relative reluctivity of material. The inverse of reluctivity is permeability (μ). In saturation condition, μ_r (B) is large and almost constant for small value of B and has nonlinear transition between these two extreme values, with B2 = $||\mathbf{B}||^2$ analytical expressions for relative reluctivity and permeability

$$\nu_r = a + \frac{(1-a)(B2)^b}{(B2)^b + c} \Leftrightarrow \mu_r = \frac{1}{a + \frac{(1-a)(B2)^b}{(B2)^b + c}} \tag{2.34}$$

where a,b and c determine to fulfills ν_r (B2=0) = a and $\lim_{B2\to\infty} \nu_{r(B2)} = 1$

2.7 Motional Effect

A large number of electromagnetic devices involve moving components, e.g. rotating and linear machines [6] (see figure 2.7). The inclusion of velocity (v) term into vector potential from equation (2.27), first we modified linear speed (v) into angular speed (ω) , angular angle (θ) and radius (r) .

$$\sigma\frac{\partial \boldsymbol{A}_z}{\partial t} + \frac{\partial}{\partial x}\left(\frac{1}{\mu_0\mu_r}\frac{\partial \boldsymbol{A}_z}{\partial x}\right) + \frac{\partial}{\partial y}\left(\frac{1}{\mu_0\mu_r}\frac{\partial \boldsymbol{A}_z}{\partial y}\right) + \sigma r\omega\left(sin\theta\frac{\partial \boldsymbol{A}_z}{\partial x} - cos\theta\frac{\partial \boldsymbol{A}_z}{\partial y}\right) = -\boldsymbol{J}_z \tag{2.35}$$

Eddy current losses in rotor and magnet, appear due the difference of the speed of magnetic field and the rotor, fundamental flux component which rotate with synchronous speed does not induce eddy current in the stator, since the air gap flux contain harmonics component, these flux have relative speed to the rotor and induce the eddy current.

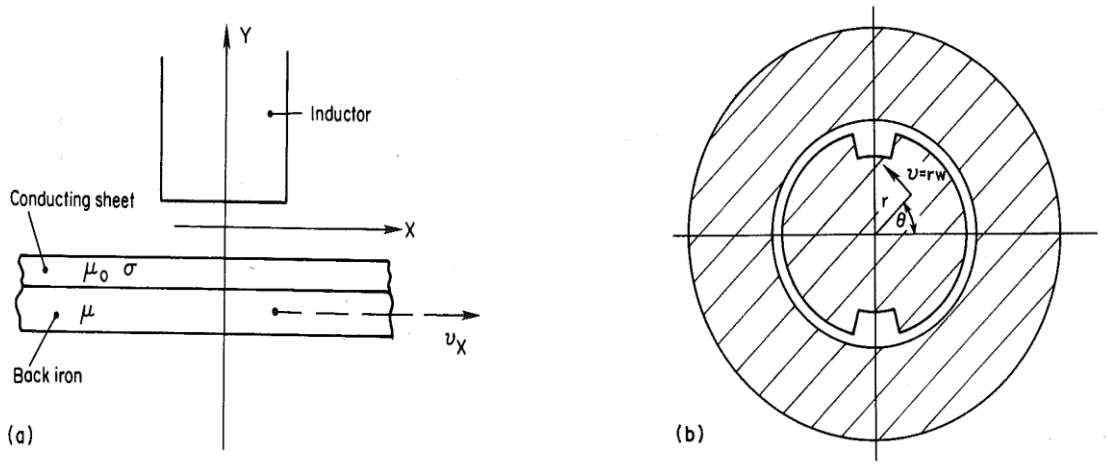

Figure 2.7 Idealized models involving motion (a) single-sided linear induction motor

(b) machine rotating with angular velocity (ω)

2.8 Electromagnetic energy

Electric energy (W_e) and magnetic energy (W_m) defined as:

$$W_e = \int_V \left(\int_0^D E.dD\right) dV = \int_V \left(\int_0^T E.\frac{\partial D}{\partial t} dt\right) dV \quad (2.36)$$

$$W_m = \int_V \left(\int_0^B H.dB\right) dV = \int_V \left(\int_0^T H.\frac{\partial B}{\partial t} dt\right) dV \quad (2.37)$$

Where V is computation domain and S is closed boundary of V, Time derivatives of energy expressed as the power of electric (P_e) and magnetic (P_m) :

$$P_e = \int_V E.\frac{\partial D}{\partial t} dV \quad (2.38)$$

$$P_m = \int_V H.\frac{\partial B}{\partial t} dV \quad (2.39)$$

These quantities in equation (2.37) and (2.38) related to resistive and radiative energy can also be expressed as the following

$$-\int_V \left(E.\frac{\partial D}{\partial t} + H.\frac{\partial B}{\partial t}\right) dV = \int_V J.EdV + \oint_S (E \times H).ndS \quad (2.40)$$

The first part of integration in right side represents resistive losses

$$P_h = \int_V J.EdV \quad (2.41)$$

The second part in right side represents radiative losses

$$P_r = \oint_S (E \times H).ndS \quad (2.42)$$

This thesis interesting with the resistive losses in magnet and back iron, since in the quasi static magnetic field, resistive losses take major part of losses compare to radiative losses.

Chapter 3

FINITE ELEMENT METHOD

This chapter will present the overview of basic theory of finite element, it will help to figure how the finite element develop into a tools to solve differential equation

3.1 Introduction

Finite element method (FEM) was proposed by Alexander Hrennikoff (1941) and Richard Courant (1942) [7], Finite element become support method to solve the differential equation due the ability to deal with complex geometries problem and non linear characteristic material.

Finite element method also have disadvantage compare to the analytical solution, however because of its numerical nature the solution is necessarily approximate. That's why if this method does not apply correctly it will lead the in accurate result.

3.2 General procedures

The summary of general recipe for finite element method [8] :

1. *Discretization* the solution domain into cells or elements
2. *Choice of the basic function*. The function v_i usually piecewise linear function to get sparse matrix.
3. *Formulation of the system* to resolve the field problem. The system of equation representing the field solution is developed by means of Galerkin's method or Rayleigh-Ritz's method)
4. *Solution of the problem*. The solution is obtained by solving the resulting system of equations.

3.2.1 Discretization domain

There are several types of element for partition (discretization)[9]. Domain Ω is domain connected to one, two or three dimensional. One dimensional, The domain is a curve and the segment is line, in the two dimensional domain, the domain is area and the segment could be in triangle and square, in the three dimensional problem the domain is volume and the element could be in tetrahedron, pyramid, prism and cube.

Generally the triangle element use for two dimensional and tetrahedron in three dimensional problem [8], figure 3.1 (a) show the different types of element and figure 3.1 (b) show the sample of discretization in 2D problem with triangle element

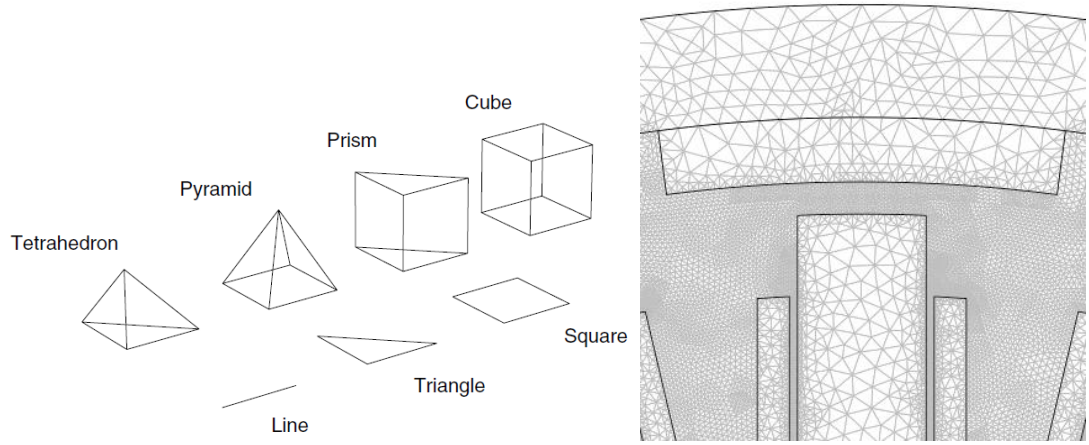

(a) (b)

3.1 (a) Different element type of discretization (b) Triangle element in 2D discretization

Output from meshing process is the table of global node number and global node coordinates, for example, let us consider 2D domain in figure 3.2, which have 4 elements and 6 nodes

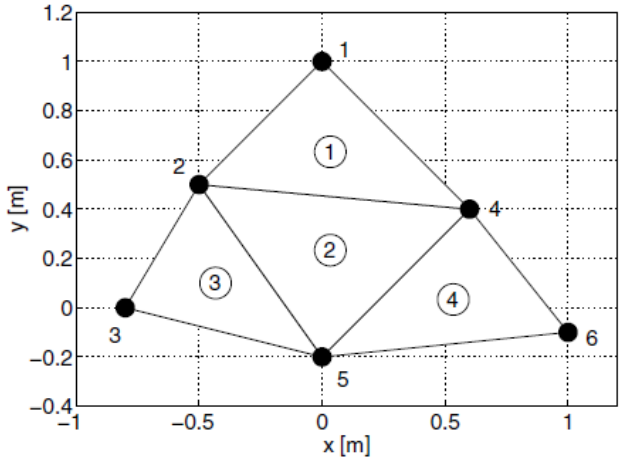

Figure 3.2 Example 2D mesh element and node

Global node coordinates for 2D mesh in figure 3.2 shown in table 3.1, and global element node show in table 3.2. This example for triangular element and the same procedure can be used for other types of element.

Table 3.1 Global nodes coordinate

Node Number / Coordinates	1	2	3	4	5	6
X	0.0	-0.5	-0.8	0.6	0.0	1.0
Y	1.0	0.5	0.0	0.4	-0.2	-0.1

Table 3.2 Global Element node

Element Number	Node Number		
1	1	2	4
2	2	4	5
3	2	3	5
4	4	5	6

3.2.1.1 Arbitrary lagrangian eulerian (ALE) mesh

To get the motion effect of rotor in our model ,the boundary of our model are moving in time, or as a function of a parameter the coordinates of each element will change in time, in finite element software package COMSOL 3.4 offered the facility to deformed mesh due the motion of physical model.

The technique for mesh movement is called an *arbitrary Lagrangian-Eulerian* (ALE) method. In the special case of a *Lagrangian* method, the mesh movement follows the movement of the physical material. Such a method is often used in solid mechanics, where the displacements often are relatively small.

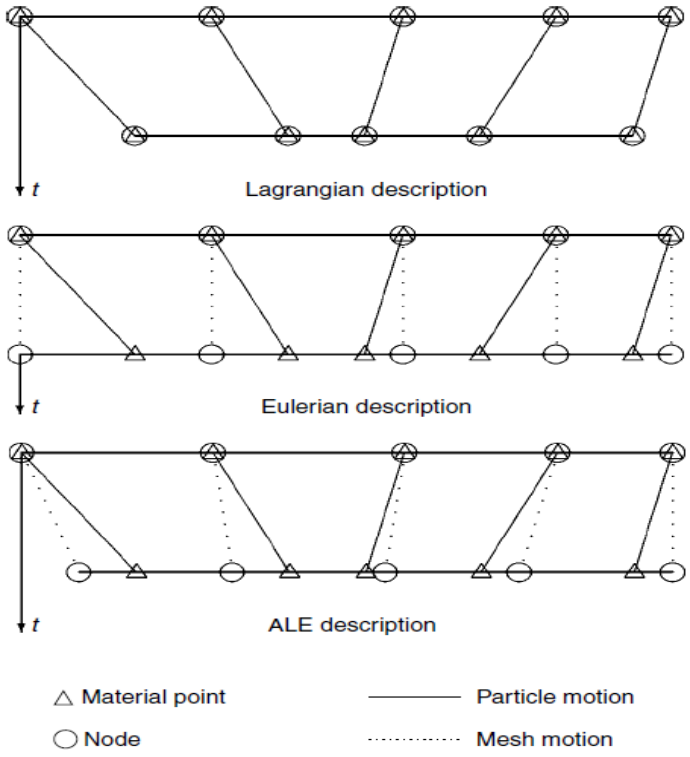

Figure 3.3 One dimensional Lagrangian, Eulerian and ALE mesh particle motion, Source [11]

When the material motion is more complicated, like in a fluid flow model, the *Lagrangian* method is not appropriate. For such models, an *Eulerian* method, where the mesh is fixed, is often used—except that this method cannot account for moving boundaries.

The ALE method is an intermediate between the *Lagrangian* and the *Eulerian* method, and it combines the best features of both—it allows moving boundaries without the need for the mesh movement to follow the material. [11], , figure 3.3 show the difference between Lagrangian and for 1 dimension particle movement, in *Lagrangian* description both of material point and mesh node point moving together, while in the *Eulerian* description material point is moving but the mesh nodal point is stationary., in the ALE description is combination between Eulerian and Lagrangian description.

3.2.1.2 Refinement mesh

Triangular elements allow for local refinement of the mesh, hence high resolution can be used where it is need, figure 3.3a and 3.b show the adaptive refinement mesh for air gap in machine model II., figure 3.4 show the comparison of relative error between adaptive refine mesh and uniform refine mesh, the figure show for the same number of element, adaptive refine mesh result the lower relative error.

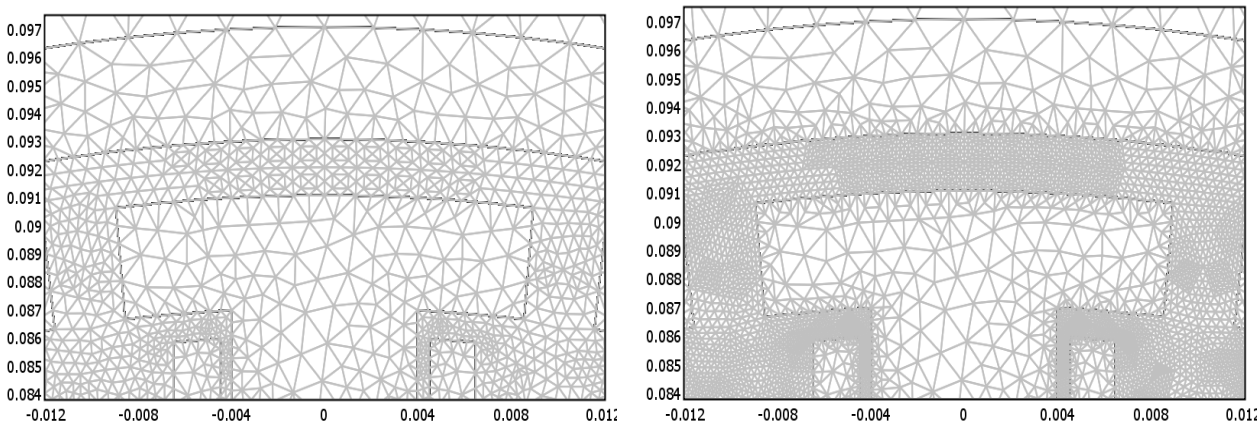

(a) (b)

Figure 3.4 Local refinements Mesh in machine Air gap (a) Before (b) After

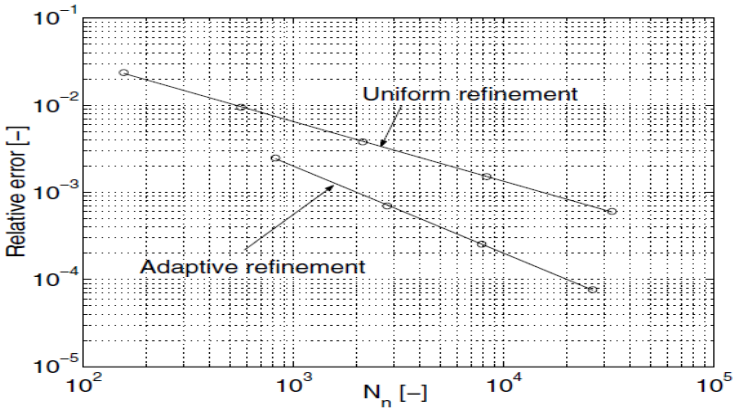

Figure 3.5 Relative error comparisons between adaptive and uniform refinement, source [7]

3.2.2 Chose the basis function

Let us assume that the structure has been divided in N_m finite element, and the total number of nodes is N_n . Each of them assumes the value Φ_i of the potential function ϕ. A linear interpolating of the function ϕ is assumed for each m-th triangular element, given by :

$$\phi_m (x,y) = a + bx + cy \tag{3.1}$$

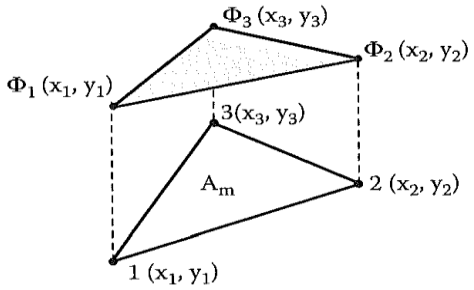

Figure 3.6 Linear interpolation of the potential function ϕ_m in m-th triangular element

In particular, in the three nodes of the triangle in (figure 3.5), the three i-th values are given by:

$$\begin{cases} \Phi_1 = a + bx_1 + cy_1 \\ \Phi_2 = a + bx_2 + cy_2 \\ \Phi_3 = a + bx_3 + cy_3 \end{cases} \tag{3.2}$$

From known value of function in the nodes of each finite element, it is possible to compute the potential in any other point of the element. If the three potential value is given, it is possible to solve the equation (3.2), the three un known parameter a,b, and c. At first it is posed area of m-th triangular element:

$$A_m = \frac{1}{2}\begin{vmatrix} 1 & x_1 & y_1 \\ 1 & x_2 & y_2 \\ 1 & x_3 & y_3 \end{vmatrix} = \frac{1}{2}[(x_2y_3 - x_3y_2) + (x_3y_1 - x_1y_3) + (x_1y_2 - x_2y_1)] \tag{3.3}$$

Using Cremer's rule

$$\begin{aligned} a &= \frac{1}{2A_m}[\Phi_1(x_2y_3 - x_3y_2) + \Phi_2(x_3y_1 - x_1y_3) + \Phi_3(x_1y_2 - x_2y_1)] \\ b &= \frac{1}{2A_m}[\Phi_1(y_2 - y_3) + \Phi_2(y_3 - y_1) + \Phi_3(y_1 - y_2)] \\ c &= \frac{1}{2A_m}[\Phi_1(x_3 - x_2) + \Phi_2(x_1 - x_3) + \Phi_3(x_2 - x_1)] \end{aligned} \tag{3.4}$$

we can substitute (3.4) into (3.1) and rewritten as

$$\begin{aligned} \phi_m(x,y) &= \left(\frac{1}{2A_m}\sum_{i=1}^{3} p_i \Phi_i\right) + \left(\frac{1}{2A_m}\sum_{i=1}^{3} q_i \Phi_i\right) + \left(\frac{1}{2A_m}\sum_{i=1}^{3} r_i \Phi_i\right) \\ &= \sum_{i=1}^{3} \frac{(p_i + q_i x + r_i y)}{2A_m} \Phi_i \\ &= \sum_{i=1}^{3} v_i(x,y)\, \Phi_i \end{aligned} \tag{3.5}$$

P_i,q_i, and r_i are constants related to equation (3.14). It is worth motice that is possible to define the function $\phi_m(x,y)$ in each point of the triangle as linear combination of the value Φ_1, Φ_2 and Φ_3 in the nodes of triangle itself,, interpolating function v_i (x,y) with i = 1,2,3 .

3.2.3 Formulation of the system

Vector field problem is generally described by differential equation defined in domain D in equation 3.6[8], where *L* is differential equation (operator), ϕ is the unknown function to be determining, and *f* is the forcing function (source). ϕ and *f* are function of positions in the space P(x,y,z) and also function of time (t).

$$L\,\phi(P,t) = f(P,t) \qquad (3.6)$$

Equation *L* can be any differential operator, in the electromagnetic problem, *L* is given by Helmholtz, Poisson or Laplace equation, within ϕ is scalar or vector field. For example in case electrostatic problem, ϕ indicates the scalar electric potential V, and its distribution is describe by Poisson equation. The forcing function is the distribution of the free charge density $f = \rho$ then equation 3.6 become: $-\text{div}(\varepsilon \text{ grad } V) = \rho$ The differential operator L is then expressed by $L = -\text{div}(\varepsilon \text{ grad})$

The field problem admits a solution not only if the differential equation that describes its distribution is known in all the points of the domain D, but also if the unknown function ϕ is given on the boundary Γ of the domain D itself and this solution is unique (unique theorem).

The condition that express the behavior function ϕ on Γ called constrain or boundary conditions. We can describe two boundary conditions:

1. Dirichlet's (Γ_1) condition, homogenous condition $\phi = 0$ on Γ_1 , non homogenous condition $\phi \neq 0$ on Γ_1 .
2. Neumann's (Γ_2) conditions, homogenous condition $\delta\phi/\delta n = 0$ or $\delta\phi/\delta n + k\phi = 0$, non homogenous condition $\delta\phi/\delta n + k\phi \neq 0$, where k is constant.

Let we take approximation function ϕ^* as approximate the unknown functionϕ, where

$$\emptyset^*(P,t) = \sum_{j=1}^{N} \Phi_j v_j(P,t) \qquad (3.7)$$

Where v_j are basis function (also called interpolating function), while Φ_j are unknown coefficients that have to be determine during computation process.

3.2.3.1 The residual method (Galerkin's method)

Residual function

$$r = L\,\phi^* - f \qquad (3.8)$$

Set to zero (or very low) in whole analysis domain, fixing weight function w_i to zero over the domain volume τ_D. This is to force the following condition:

$$R_i = \int_{\tau_d} w_i(L\phi^* - f)d\tau = 0 \quad (3.9)$$

Weight function in Galerkin's method w_i are chosen equal to interpolating function v_i , equations 3.7 and 3.4 form equations

$$R_i = \int_{\tau_d} v_i L\left(\sum_{j=1}^{N} \Phi_j v_j\right) - v_i f \; d\tau = 0 \quad i = 1,2,3 \ldots N \quad (3.10)$$

This equation yield to a system equation that can be expressed as

$$[SS][\phi] = [T] \quad (3.11)$$

Where $[\phi]$ is the column vector of unknown coefficients Φ_i. [SS] is a matrix vector depend on basic function, the elements of these matrix are given by:

$$s_{ij} = \frac{1}{2}\int_{\tau_d}\left(v_i L v_j + v_j L v_i\right) d\tau \quad (3.12)$$

[T] Is column vector, the elements of these matrixes given by:

$$t_i = \int_{\tau_d} v_i f \; d\tau \quad (3.13)$$

3.2.3.2 The variational method (Rayleigh-Ritz's method)

The variational method solves the field problem by means of an integral approach, starting from the differential equations (3.6) , a proper functional is built, in certain ways that its minimum corresponds to the solution of the field problem, which is when field in equation (3.6) and the boundary conditions have been matched.

This function is just called variational; the process of seeking the solution of differential problem becomes then a process of seeking the minimum of the functional. Equation (3.6) can be expressed as

$$F(\phi) = \frac{1}{2}\langle L\phi, \phi\rangle - \frac{1}{2}\langle \phi, f\rangle - \frac{1}{2}\langle f, \phi\rangle \quad (3.14)$$

The function of ϕ is substituted by ϕ^* from equation (3.7), where v_i are defined in the whole domain D. by substituting equation (3.7) to (3.15), and posing to zero the derivatives of the variational F with respect to the unknown coefficient Φ_j

$$\frac{\delta F}{\delta \Phi_j} = 0 \quad i = 1,2,3,..N \quad (3.15)$$

A system of linear equations, similar to equation (3.11), matrix vector [SS] is symmetrical and the system is identical to that obtained by the residual Galerkin's method. The functional is given by

$$F(\emptyset^*) = \sum_{m=1}^{M} F(\emptyset_m^*)$$
$$= \sum_{m=1}^{M}\left[\frac{1}{2}\int_{\tau} \emptyset_m^* L \emptyset_m^* d\tau - \frac{1}{2}\int_{\tau} f_m \emptyset_m^* d\tau\right] \quad (3.16)$$

That in matrix form result

$$F(\phi^*) = \tfrac{1}{2}\,[\phi]^t\,[SS][\phi] - [\phi]^t[T] \quad (3.12)$$

To solve the field problem, the value of Φ_{mj} have to compute in the nodes of each element. It is necessary to prepare a system of equations, whose solution corresponds to the values of $\Phi_{mj.}$ In case of Galerkin's method, in the m-th of element, the n-th integral given by equation (3.10)and in case of Rayleigh-Ritz's method, function given by equation (3.16).

3.3.4 The problem's solution

Once the system is assembled, including of the essential boundary conditions, it is still in the form of equation (3.11). The system is solved by one of the common numerical methods, among them :

1. The Gauss-Jordan direct method. This method is applied when the physical properties are linear, which when all the parameters of the materials are constants.
2. The Newton-Rapson iterative method. This method is applied when the materials are not linear, which when the parameter of material are not constant but they are function of the value of magnitude of the magnetic fields. The common case is th B-H curve of ferro magnetic materials presents in chapter 2.

Chapter 4

ANALYTICAL CALCULATION OF EDDY CURRENT LOSSES IN THE BACK IRON AND PERMANENT MAGNET

This chapter will present the analytical calculation of eddy current losses in permanent magnet and back iron. The machines consist of three models, based on master volt machine which have been manufactured.

The analytical method is based on method which was presented in..[12,13] for calculating eddy current in back iron, and [14,15] for calculating eddy current in magnet.

4.1 Machine description

The three machines which were analyzed in this chapter are 3 phase machines. The winding is a fractional pitch concentrated winding with permanent magnet excitation. Figure 4.1 shows the machine stator and rotor configuration: machine I and II consist of 27 teeth and 19 Poles. Machine I has open slots and machine II has semi closed slots, machine III has 27 teeth and 24 pole combination. A complete description of these machines is written in table 4.1and4.2.

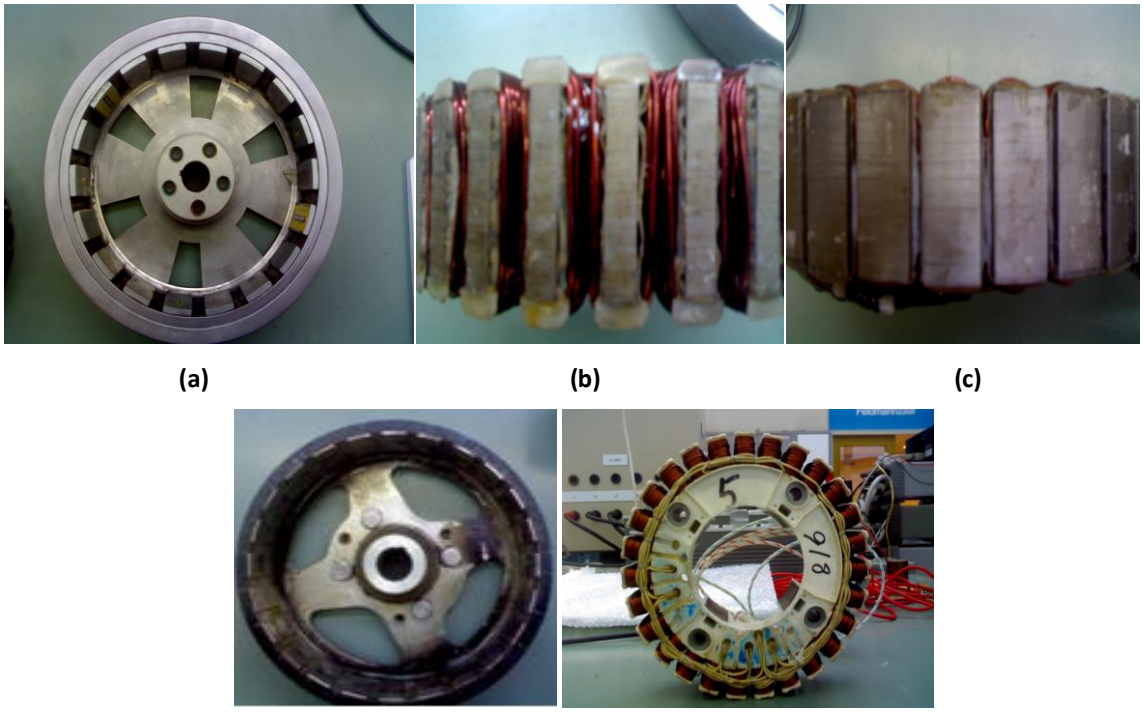

(a) **(b)** **(c)**

(d) **(e)**

Figure 4.1 (a) Machine I and II rotor (b) Machine I stator (c) Machine II Stator (d) Machine III rotor (e) Machine III stator

Table 4.1 Machine Dimensional Parameters

Parameter	Description	Machine I	Machine II	Machine II
N_t	number of tooth	27	27	27
N_p	number of pole	18	18	24
N_c	number of turn each coil	15	15	58
r_s	air gap radius	91 mm	91 mm	79 mm
r_{si}	inner radius stator	46 mm	46 mm	51 mm
h_s	slot height	30 mm	26 mm	16 mm
h_{so}	slot height open		4 mm	2 mm
b_t	tooth width	8 mm	8 mm	5 mm
b_{tt}	tooth width with edges		18 mm	14 mm
h_{sy}	height of stator yoke	10 mm	10 mm	10 mm
τ_s	sloth pitch	21.17 mm	21.17 mm	18.4 mm
l_g	air gap length	2 mm	2 mm	2 mm
r_m	permanent magnet surface radius	93 mm	93 mm	81 mm
l_m	magnet length	4 mm	4 mm	2 mm
b_p	magnet width	24 mm	24 mm	13.9 mm
l_s	stack length	56 mm	56 mm	41 mm
Rated Current		5 A	5 A	2.1 A
Rated Speed		3600 rpm	3600 rpm	3600 Rpm
Rated Power		9 kW	9 kW	3 kW

The electric and magnetic properties of machine material which are used in analytical calculation and Finite element calculation are shown in table 4.2, these values have been taken from [12] and [14].

Table 4.2 Material properties

Parameter	Description	Value
ρ_{fe}	back iron resistivity	$2x10^{-7}$ Ω.m
ρ_m	magnet resistivity	$1.3 x10^{-6}$ Ω.m
B_{rm}	magnet remanent flux density	1.2 T
μ_{rfe}	relative permeability back iron	200
μ_{rm}	relative permeability magnet	1.05

4.2 Analytical calculation for Eddy current losses in back iron

The method to calculate eddy current losses in rotor back iron permanent magnet machine is presented in [12, 13]. These methods have simplifying assumptions:

1. Stator teeth and slot are replaced by a smooth surface placed at a distance g_{eff} from the back iron.
2. Flux crosses the air gap perpendicularly
3. Current are sinusoidal and in phase with EMF
4. Stator permeability and resistivity are both infinite

The first step of this method is to determine the flux density in the air gap due to stator currents. The flux density is calculated by assuming that one phase is conducting current while the other phases are having no current. Using ampere's law we can get the flux magnitude in the air gap as a function of position. The next step is to write the flux density in the form of a Fourier series to get the magnitude of space harmonic flux density. After the magnitude is calculated, the relative speed can also be calculated. The final step using equation 4.11 for getting eddy current losses in the back iron.

4.2.1 Modeling space harmonic of winding

The flux density with fundamental wave (λ_1) and stator coordinate (x_s), have general a Fourier series as shown in 4.1, We chose the position of x_s =0 in such way the density flux function is even, which will make the dc offset and the sinus function in the Fourier series to disappear so the remaining flux density function will consist of the cosines part :

$$B_{sa}(x_s) = \sum_{k=1}^{\infty} \hat{B}_{sk} \cos\left(k \frac{2\pi x_s}{\lambda_1}\right) \qquad (4.1)$$

Flux density contribution from other phase can also be expressed using the same way as 4.1 and having a different phase of 2π /3. Assuming that the current is pure sinusoidal and having positive sequence abc and angular frequency ω, then the flux density can be written as

$$B_{sa}(x_s) = \sum_{k=1}^{\infty} \hat{B}_{sk} \cos\left(k \frac{2\pi x_s}{\lambda_1}\right) \cos(\omega t)$$

$$B_{sb}(x_s) = \sum_{k=1}^{\infty} \hat{B}_{sk} \cos\left(k \frac{2\pi x_s}{\lambda_1} - {}^{2\pi}/_{3}\right) \cos\left(\omega t - {}^{2\pi}/_{3}\right)$$

$$B_{sb}(x_s) = \sum_{k=1}^{\infty} \hat{B}_{sk} \cos\left(k \frac{2\pi x_s}{\lambda_1} - {}^{4\pi}/_{3}\right) \cos\left(\omega t - {}^{4\pi}/_{3}\right) \qquad (4.2)$$

The total flux density in the air gap is the sum of the three phase flux density $B_s = \sum_{k=1}^{\infty} B_{sk}$

Where:

$$B_{sk} = \frac{3}{2} \hat{B}_{sk} \cos\left(k \frac{2\pi x_s}{\lambda_1} - \omega t\right) \; for\; k = 1,4,7..$$

$$B_{sk} = \frac{3}{2} \hat{B}_{sk} \cos\left(k \frac{2\pi x_s}{\lambda_1} + \omega t\right) \; for\; k = 2,5,8...$$

$$B_{sk} = 0 \; for \; k = 3,6,9.. \tag{4.3}$$

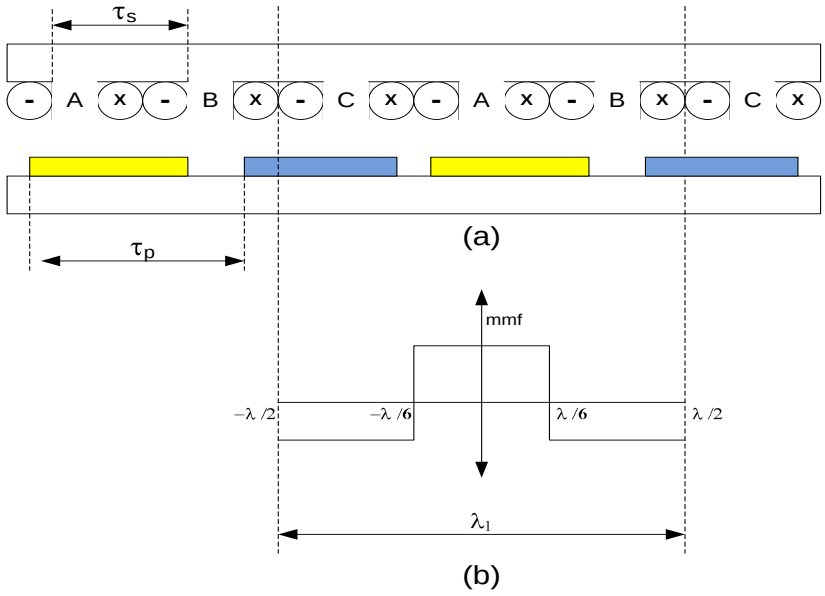

Figure 4.2 (a) Machine I and II winding arrangement (b) Air Gap MMF due current in phase A

4.2.1.1 Machine I and II

The slot pole combination of Machine I and II is 27 slot 18 pole, the fractional pitch winding with 3 tooth,3 coil, 2 pole is shown in figure 4.2(a), Let us consider that only in phase A the current is conducting, then the MMF is shown in figure 4.2(b), with N is the number of turn in one coil, i_a is the rms current of phase a, g_{eff} is the air gap length multiplied by carter factor. The magnitude of MMF calculated from ampere law, and the flux density become:

$$B_{sa=}\begin{cases} \frac{2\mu_0 N i_a}{3 g_{eff}} \; for & -\frac{\lambda_1}{6} < x_s < \frac{\lambda_1}{6} \\ -\frac{\mu_o N i_a}{3 g_{eff}} \; for & -\frac{\lambda_1}{2} < x_s < -\frac{\lambda_1}{6} \\ & \frac{\lambda_1}{6} < x_s < \frac{\lambda_1}{2} \end{cases} \tag{4.4}$$

Fourier series from equation 4.1 gives the magnitude of the space harmonic of flux density

$$\hat{B}_{sk} = \frac{2\mu_0 N i_a}{k\,\pi\, g_{eff}} \sin\left(\frac{k\pi}{3}\right) \tag{4.5}$$

4.2.1.2 Machine III

The slot pole combination of Machine II is 27 slot 24 pole, the fractional pitch winding with 9 tooth 9 coil, 8 pole is show in figure 4.3(a). The MMF generated due the current in phase A is shown in figure 4.3(b), the flux density become

$$\frac{10\mu_0 N i_a}{9\, g_{eff}} \quad for \quad -\frac{\lambda_1}{18} < x_s < \frac{\lambda_1}{18}$$

$$B_{sa} = -\frac{8\mu_0 N i_a}{9\, g_{eff}} \quad for \quad \begin{matrix} -\frac{\lambda_1}{6} < x_s < -\frac{\lambda_1}{18} \\ \frac{\lambda_1}{18} < x_s < \frac{\lambda_1}{6} \end{matrix}$$

$$\frac{\mu_0 N i_a}{9\, g_{eff}} \quad for \quad \begin{matrix} -\frac{\lambda_1}{2} < x_s < -\frac{\lambda_1}{6} \\ \frac{\lambda_1}{6} < x_s < \frac{\lambda_1}{2} \end{matrix} \tag{4.6}$$

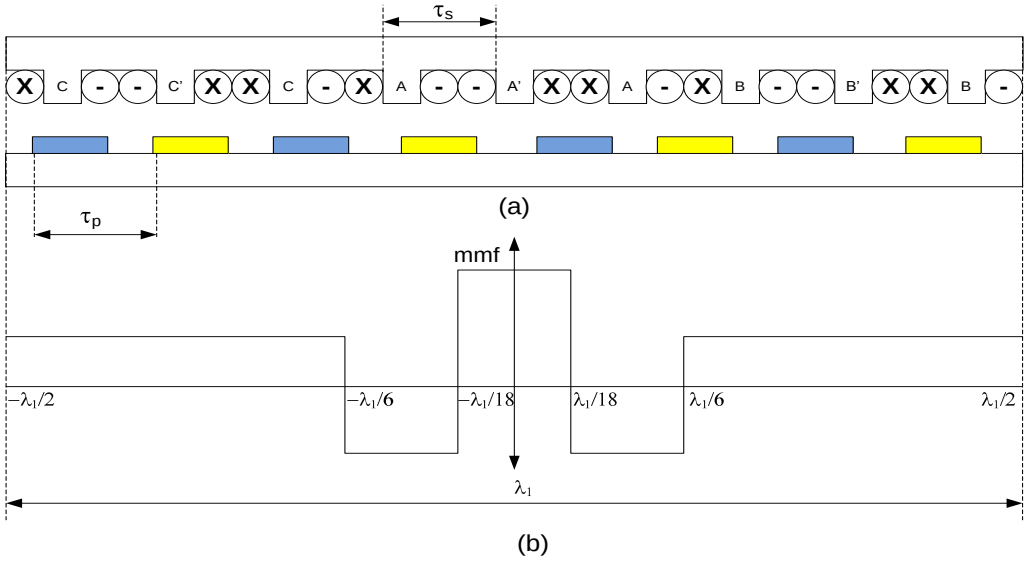

Figure 4.3 (a) Machine III winding arrangement (b) Air Gap MMF due to current in phase A

From equation 4.3, magnitude of the space harmonic of the flux density is

$$\hat{B}_{sk} = \frac{2\mu_0 N i_a}{k\,\pi\, g_{eff}} \left(2 \sin\left(\frac{k\pi}{9}\right) - \sin\left(\frac{k\pi}{3}\right) \right) \tag{4.7}$$

From equation 4.5 and 4.7 we can plot the magnitude of air gap flux for the three machine models, Figure 4.4 shows that winding arrangement of machine III contains much higher flux harmonic amplitude compared to machine I and II. It is clear that machine III predicted will produce much higher losses compared to machine I, and II for the same number of turn and rate current. But the advantages of winding in machine III is that it has higher winding factor compare to machine I and II.

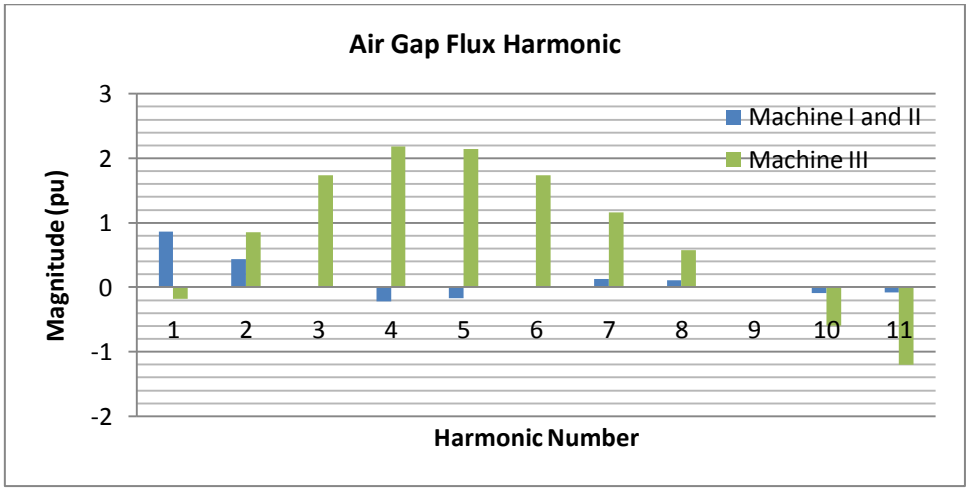

Figure 4.4 Comparison Magnitude of Flux Harmonic

4.2.2 Translator speed

To get the relative speed of translator to the flux density space harmonic we can transform the coordinate from stator to rotor can be transformed as follows

$$X_s = X_r \mp v\,t = X_r \mp \frac{\omega\tau_p}{\pi}t = X_r \mp \frac{\omega\lambda_1}{2p_\lambda\,\pi} \tag{4.8}$$

Where X_r is the rotor coordinate, v is linear speed of the translator and p_λ is the number of pole pair within the wave length λ_1., + sign is used if the phase order is abc (+) and – sign is used if the phase order is acb (-). Substituting the equation 4.8 to 4.3 and the following equation is obtained

$$B_{sk} = \frac{3}{2}\hat{B}_{sk}\cos\left(k\frac{2\pi x_r}{\lambda_1} + \left(\frac{k}{p_\lambda} - 1\right)\omega t\right)\ for\ k = 1,4,7..$$

$$B_{sk} = \frac{3}{2}\hat{B}_{sk}\cos\left(k\frac{2\pi x_s}{\lambda_1} + \left(\frac{k}{p_\lambda} + 1\right)\omega t\right)\ for\ k = 2,5,8... \tag{4.9}$$

$$B_{sk} = 0\ for\ k = 3,6,9..$$

By choosing the position when flux density is maximum as the reference point, the relative speed of space harmonic becomes

$$v_r = -\frac{\left(\frac{k}{p_\lambda}-1\right)}{k}\frac{\lambda_1\omega}{2\pi}\ \ for\ k = 1,4,7$$

$$v_r = -\frac{\left(\frac{k}{p_\lambda}+1\right)}{k}\frac{\lambda_1\omega}{2\pi}\ \ for\ k = 2,5,8 \tag{4.10}$$

4.2.3 Losses calculation and Result

Using equation in [18] eddy current losses per square meter surface area is given by

$$P_A = \frac{\hat{B}_o{}^2 v^2 \delta}{4\rho_{Fe}} \tag{4.11}$$

Where $\hat{B}_o$ is the amplitude of flux density, *v* is the relative speed of flux density wave to translator and δ is the skin dept given by

$$\delta = \sqrt{\frac{2\rho_{Fe}}{\mu_0\mu_{fe}\omega}} \tag{4.12}$$

For the rated current and speed of, Table 4.3 gives the calculation result for 3 machines

Table 4.3 Back iron eddy current Losses calculation at rated speed and current

Harmonic Number	**1**	**2**	**3**	**4**	**5**	**6**	**7**	**8**	**9**	**10**	**11**
					Flux Amplitude(mT)						
Machine I	184	29	0	-46	-5	0	26	2	0	-18	-1
Machine II	226	36	0	-56	-6	0	32	2	0	-22	-1

Machine III	-19	21	0	72	58	0	6.1	-2.3	0	1.8	-3.9	
					Relative Speed (m/s)							
Machine I	0	-51	0	-26	-41	0	-29	-39	0	-31	-37	
Machine II	0	-48	0	-24	-39	0	-27	-36	0	-30	-35	
Machine III	89	-89	0	0	-54	0	-13	-45	0	-18	-41	
					Losses (watt)							**TOTAL**
Machine I	0	38.28	0	23.51	0.44	0	7.07	0.05	0	3.1	0.11	74.14
Machine II	0	49	0	30	0.6	0	9.1	0.1	0	4	0	110.53
Machine III	49.8	46.7	0	0	98.6	0	0.09	0.09	0	0.012	0.19	201.68

Table 4.3 shows that machine I and II have lower losses compared to machine III, The higher losses in machine II caused by the higher harmonic frequency in the air gap flux density at machine III. Compared to machine I, machine II has higher eddy current losses than machine II, because the semi close slot at machine II produces lower effective air gap (g_{eff})and as result it produces the higher amplitude of harmonic air gap.

In reality, higher amplitude of air gap also produces higher EMF, In order to get the same EMF, machine II can have less number of turn compared to machine I. In this calculation the number of turn for machine I and II is equal. It makes the difference by making losses calculation of Machine I and II to be influenced only by geometrical properties.

Variation of permeance between open slot and semi closed slot will affect the difference in losses caused by the harmonic space. One way to see the effect of slotting on the losses is by calculation using finite element.

Figure 4.5 shows the variation of eddy current losses in back iron as a function of variable of speed by keeping the current constant at the rated value. It can be seen clearly at higher speed, the losses also rise to higher value. Figure 4.6 shows eddy current losses as function of phase current. Machine III shows the highest losses compared to machine I and II, but machine II has the highest winding factor, which make capability to produce high voltage with lower number of turn.

The balance between reduced copper losses due to lower number of turn and the rise of back iron losses probably would become interesting option to determine the choice of slot/pole combination and winding arrangement of the machine.

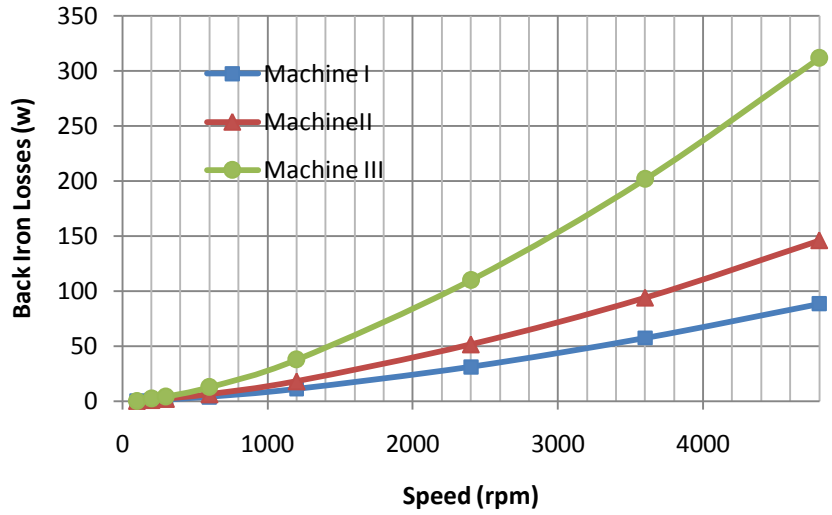

Figure 4.5 Variation of back iron loss with rotor speed at rated current

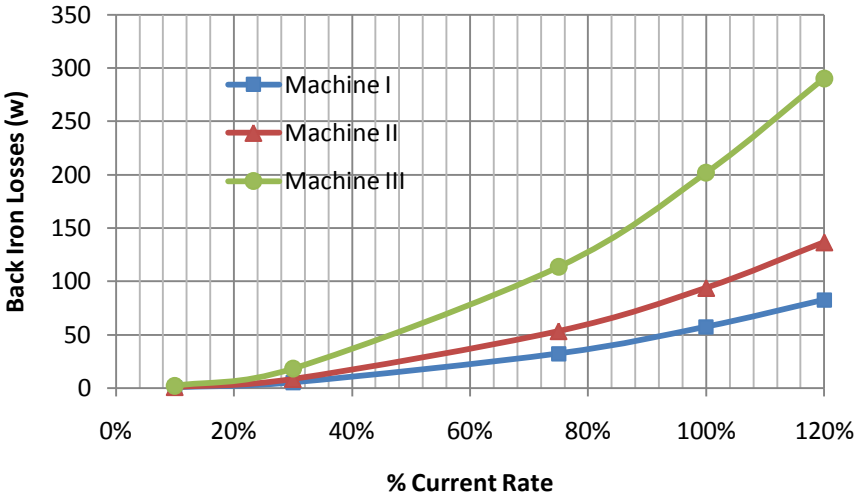

Figure 4.6 Variation of back iron loss with current at rated speed

4.3 Analytical calculation for Eddy current losses in magnet

Rare earth magnet has relatively high conductivity [14,15] , the value of 0.5 and 1.5 μΩm, for the machine which work at high speed, the magnet losses should be taken into account due to the risk of demagnetization.

Analytical solution for eddy current losses in magnet is presented in [14] and [15]. The following assumptions are taken in this method :

1. The stator and rotor have zero electrical conductivity and infinite permeability.
2. The induced eddy current are aimed at axially only, the end effect are neglected.
3. The air gap permeance variation due to the slotting is neglected.
4. Magnet relative permeability is one.
5. Stator current is pure sinusoidal

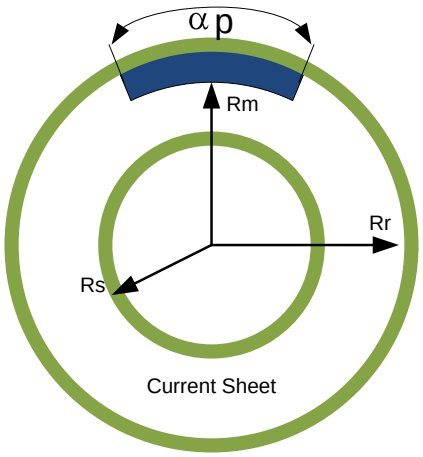

Figure 4.7 Analytical Model for external rotor

The model is formulated in two dimensional polar coordinates, stator winding is represented by equivalent current sheet Js (shown in figure 4.7), which refer to the rotor reference :

$$J_{s=}\begin{cases}\frac{q}{2}\sum_n J_n\cos\left(np_s\emptyset_r - p_r\omega t\right), & for\ n = qk + m\\ \frac{q}{2}\sum_n J_n\cos\left(np_s\emptyset_r + p_r\omega t\right), & for\ n = qk - m\\ 0, & for\ n \neq qk \mp m\end{cases} \quad (4.14)$$

Where m = ± 1, n is space harmonic order p_r is number of pole magnet pair, p_s is fundamental pole pair associated with stator winding, $J_n = (2N_sI_m/\pi Rs)xK_{sov}\ K_{wn}$, K_{wn} is the winding factor $K_{wn} = \sin^2(nP_r\pi/N_s)$, N_s is number of series conductor, $K_{sov} = 1/K_{carter}$.

Take vector potential A (r,α) where $\nabla^2 A = 0$ and the general solution becomes

$$A(r,\alpha) = \sum_n^{\infty}(C_n r^{np_s} + D_n r^{-np_s})\cos\left(np_s\alpha\right) \quad (4.15)$$

Radial and tangential component of the magnetic flux are expressed as

$$B_r = \frac{1}{r}\frac{\partial A}{\partial \alpha} \quad \text{and} \quad B_\emptyset = -\frac{\partial A}{\partial r} \quad (4.16)$$

Coefficient C_n and D_n can be obtain from the boundary conditions

$$B_\emptyset\big|_{r=R_r} = 0 \quad \text{and} \quad H_\emptyset\big|r = +_{R_s} - H_\emptyset\big|r = -_{R_s} = J_s \quad (4.17)$$

Transforming to rotating reference frame by changing $\alpha = \emptyset_r + \omega_{rt}$, the induced eddy current density in permanent magnet is then given by

$$J_m\left(r, \emptyset_{r,t}\right) = -\frac{1}{\rho}\frac{\partial A(r,\emptyset_r,t)}{\partial t} + C(t) \quad (4.18)$$

C(t) is the integration constant which guarantee that the net total current flow in each segment is zero

$$\int_{R_m}^{R_r}\int_{-\alpha_p/2}^{-\alpha_p/2} J_m r dr d\emptyset_r = 0 \quad (4.19)$$

And the average induced eddy current losses in magnet is derived as:

$$P = \frac{\omega}{2\pi}\int_0^{2\pi/\omega}\int_{-\alpha p/2}^{\alpha p/2}\int_{Rm}^{Rr}\rho_m {J_m}^2 r dr d\theta_r dt \quad (4.20)$$

Total eddy current losses in magnet per axial length is write down in here:

$$P = \sum_{n=1}^{\infty}(P_{cn} + P_{an})(W/m) \tag{4.21}$$

Where:

$$P_{cn} = \frac{9\mu_0\alpha}{8\rho_m}\frac{{J_n}^2}{n^2{p_s}^2}(np_s \pm p_r)^2\omega^2 \times \left[\left(\frac{Rm}{Rs}\right)^{2np_s}\frac{Rs^2Rm^2}{(2np_s+2)} + \left(\frac{Rr}{Rs}\right)^{2np_s}Rs^2Rm^2F_n + \left(\frac{Rr}{Rs}\right)^{2np_s} \times Rs^2(Rm^2 - Rr^2)\right] / \left[1 - \left(\frac{Rr}{Rs}\right)^{2np_s}\right]^2 \tag{4.22}$$

$$F_n = \begin{cases} \frac{\left(\frac{Rm}{Rs}\right)^{-2np_s+2}-1}{-2np_s+2} & for\ np_s \neq 1 \\ \ln\left(\frac{Rm}{Rr}\right) & for\ np_s = 1 \end{cases} \tag{4.23}$$

$$P_{an} = -\frac{9\mu_0\alpha}{\alpha\rho_m}\frac{{J_n}^4}{n^4{p_s}^4}(np_s \pm p_r)^2\omega^2 \times \left[R_s{R_r}^2G_n\left(\frac{Rr}{Rs}\right)^{np_s} + \left(\frac{Rs}{Rr}\right)^{2np_s}\frac{RsRr^2}{(np_s+2)}\left(1 - \left(\frac{Rr}{Rm}\right)^{2np_s+2}\right)\right] \times \frac{sin^2\left(np_s\frac{\alpha}{2}\right)}{(Rr^2 - Rm^2)\left(1-\left({Rr}/{Rs}\right)^{2np_s}\right)^2} \tag{4.24}$$

$$G_n = \begin{cases} \frac{\left(\frac{Rm}{Rs}\right)^{-2np_s+2}-1}{-np_s+2} & for\ np_s \neq 2 \\ \ln\left(\frac{Rm}{Rr}\right) & for\ np_s = 2 \end{cases} \tag{4.25}$$

± sign in equation related to(-) if n= 1,4,7…., and (+) for n = 2,5,8., refer data from table 4.1and 4.2, we calculate the predictions of magnet losses, for rated speed and current. The predicted losses in the magnet are shown in table 4.4

Table 4.4 Magnet eddy current Losses calculation at rated speed and current

Harmonic Number/ Magnet Losses	1	2	3	4	5	6	7	8	9	10	Total Losses (w)
Machine I	1.01	2.26	0	2.17	31.11	0	5.55	49.52	0	0.09	92.27
Machine II	1.80	4.25	0	4.18	41.72	0	11.6	97.97	0	0.25	141.45
Machine III	0.05	0.09	0	0.64	54.72	0	11.62	48.24	0	-9.4	105.98

Figure 4.6 shows the increase of losses related to the speed. From this condition, over rated speed of the machine will be hazardous to the magnet because the increase of losses will raise the temperature of the magnet. From equation 4.20-4.25 we can predict a number of factors which influence eddy current losses in magnet such as air gap length, magnet thickness, and magnet pole arc. Refer to [18]. One of the effective ways to reduce magnet losses is by segmenting the magnet.

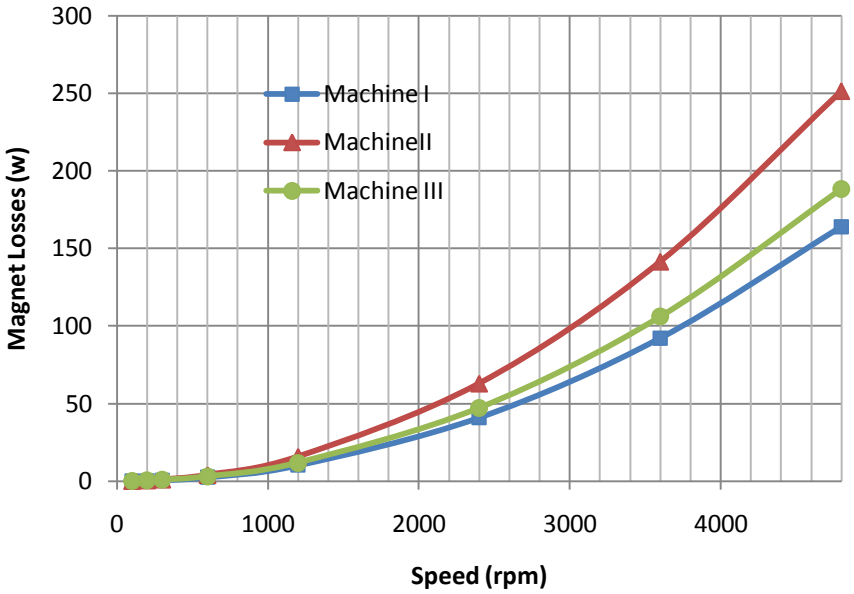

Figure 4.8 Variation of Magnet losses with rotor speed at rated current

It is shown in figure 4.6 and 4.7, losses in machine I and II much higher than machine III, the main factor is the volume of the magnet in machine I and II much higher than magnet in machine III, machine I and II design as flywheel

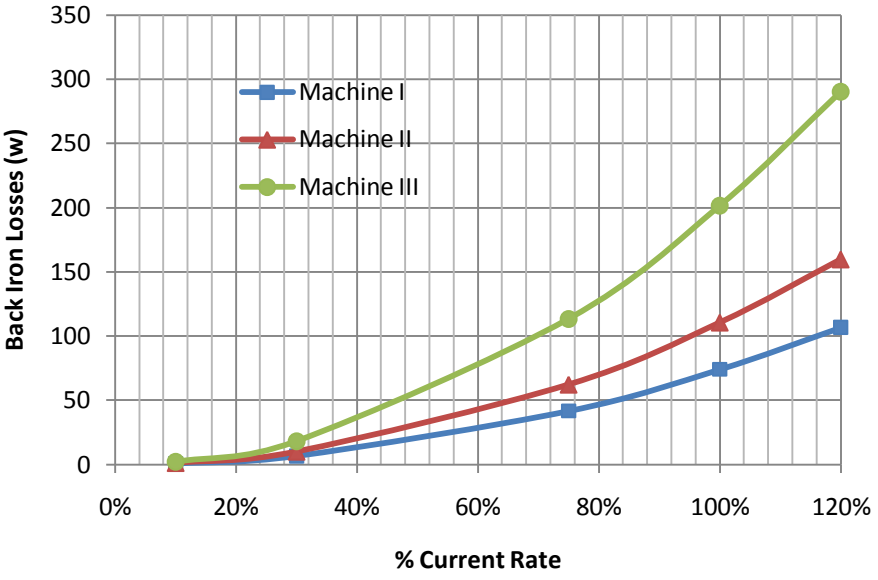

Figure 4.9 Variation of Magnet losses with current load at rated speed

Chapter 5

FINITE ELEMENT CALCULATION OF EDDY CURRENT LOSSES IN BACK IRON AND PERMANENT MAGNET

This chapter will present the Finite Element Method (FEM) for the calculation of eddy current losses in back iron and permanent magnet. The simulation will be run using finite element package software Comsol Multiphysics.

5.1 Simulation setup

The complete process of simulation process consists of three parts: preprocessing process, solver process and post-processing process.

During preprocessing process environmental conditions for simulation are prepared such as : geometrical data, material properties, excitation source and boundary conditions using data in table 4.1 and 4.2 for the geometrical data and material properties.

Meshing process is one of the important steps to get better accuracy from the computation, but it also result in longer time consumption for the computation process if we chose to use small size elements for the whole model. To deal with accuracy and computation time, a particular area which is more sensitive toward the change of variable is chosen. In our model, air gap is the area that should have a better accuracy. In this simulation we use 8 layers air gap mesh to get better accuracy, since the size of the element in this area is around 0.25 mm, the number of total elements for this condition around 150.000-200.000. Figure 5.1 shows meshing result for machine 1 with 8 layers mesh in the air gap.

Three boundary conditions are used for these simulations:

1. *Surface current boundary* .Normal component of magnetic field H in this boundary is expressed by n x ($\mathbf{H}_1$-$\mathbf{H}_2$) = J_{sz}. it is assumed that all of the current flow (in z direction) only in the surface of conductor
2. *Magnetic insulation boundary*, the magnetic vector potential in component z, is expressed as A_z=0, in there is no flux in or out of this boundary.
3. *Continuity boundary*, normal component of magnetic field **H** in this boundary is expressed by n x ($\mathbf{H}_1$-$\mathbf{H}_2$) = 0.

In solver setting the simulation time is set to 2T, where T is current period. The time step was also limited to 3.7 x 10^{-5} second for getting just quite enough accuracy. Simulation for 3600 rpm rotor speed was carried out in 100 steps time. Simulation time is 1/270 second (one period is 1/540 second). Another setting for the solver is absolute tolerance. This value will determine the iteration

process error. Since in this simulation potential vector magnetic A_z is the most important value for other calculation, the absolute tolerance for A_z is set to be $1x10^{-6}$.

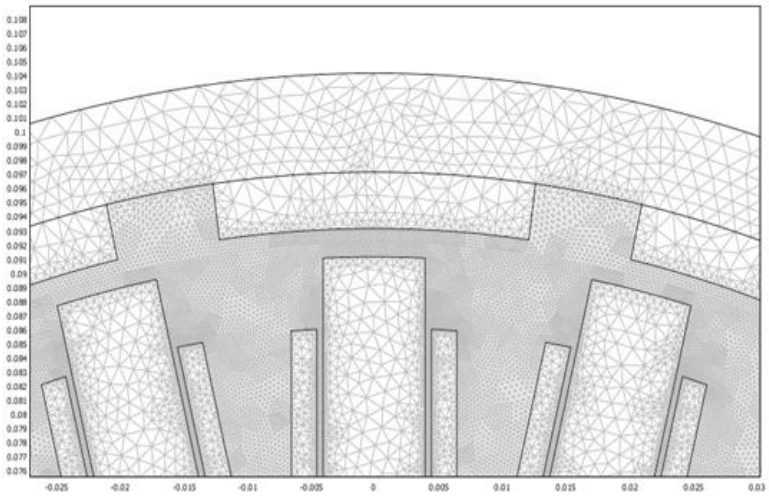

Figure 5.1 Meshing result for machine I

The last process in simulation is post-processing process. In this step the information needed is being extracted after having solved the differential equations. In our case, after the we get magnetic potential A_z in each position and time, other important variables can be extracted, such as flux density, induced current density and resistive heating (losses).

5.2 Simulation Result

5.2.1 Machine I

Time consumed for this simulation around 15-20 minutes for each current and speed conditions. For instantaneous time t = 2T figure 5.2 (a) shows the flux density in normal direction, In the sharp area, for example, in the corner of the tooth, the concentration of flux density is much higher than in the other area, The maximum value flux density reaches 4.6 T because this simulation linear material properties are being used. In other words there is no saturation effect.

Figure 5.2 (b) shows the distribution of induced current (eddy current) and figure 5.2 (c) shows the distribution from resistive heating (losses) in the back iron and magnet. Since it was assumed that the stator have zero conductivity, the eddy current losses only appear in the back iron and magnet.

The losses are obtain from integrating surface resistive heating over the area then multiplied by axial length of the machine, and calculating the average value in one period of time. Figure 5.2 (c) concentrations of losses in back irons appear mostly on the surface areas near the magnet, these areas also have the highest concentration of flux density and induced current. Induced current level for this condition reaches a maximum level $9x10^6$ A/m^2, and while resistive heating could reach 1,6 x 10^7 W/m^3.

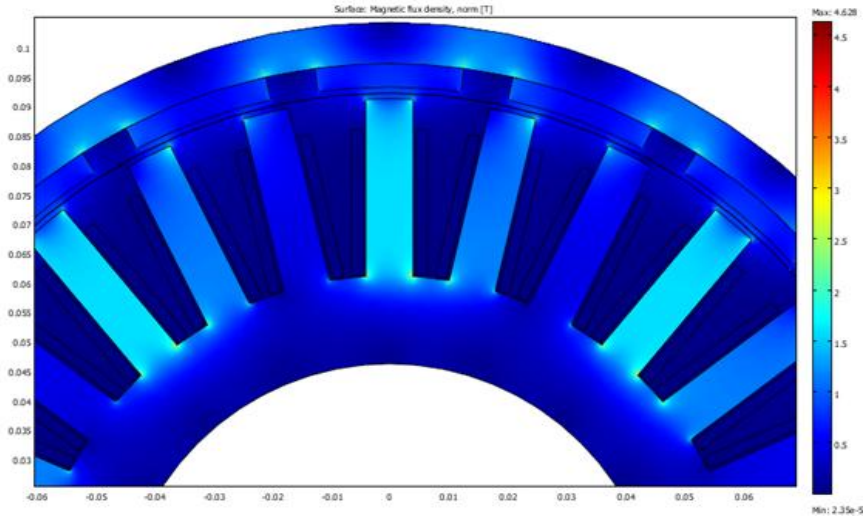

(a) Flux density

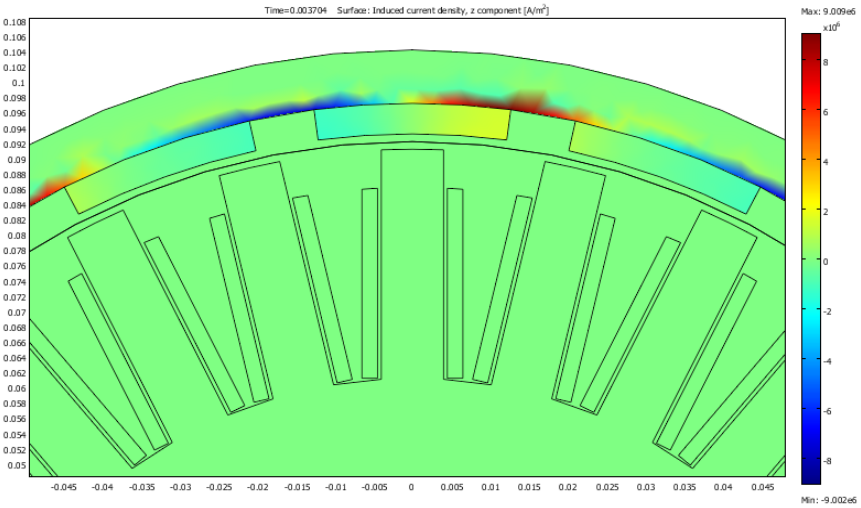

(b) Induced current density

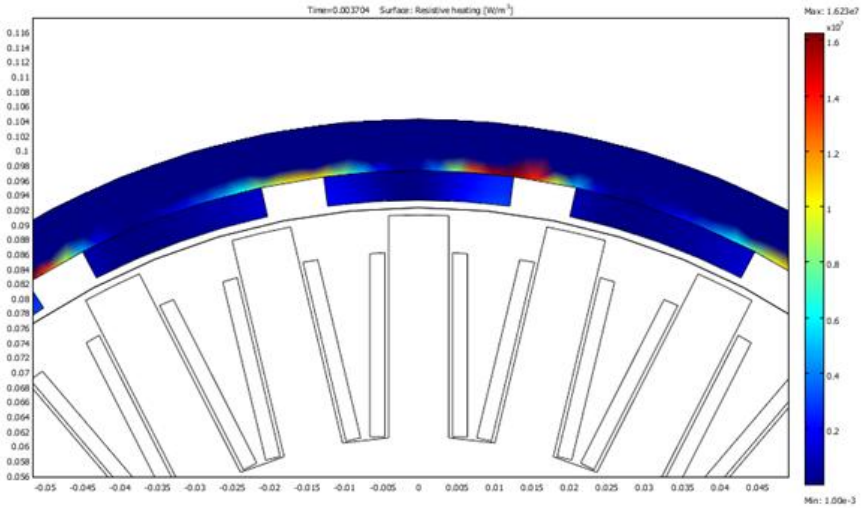

(c) Resistive heating

Figure 5.2 Instantaneous condition machine I at t = 2T

5.2.1.1 Variation of losses with rotor speed

For this simulation, the stator current (Is) is kept at a constant value 5 A rms, and the rotor speed varying from 600 to 4800 rpm. Losses for magnet and back iron are shown in figure 5.3 and table 5.1

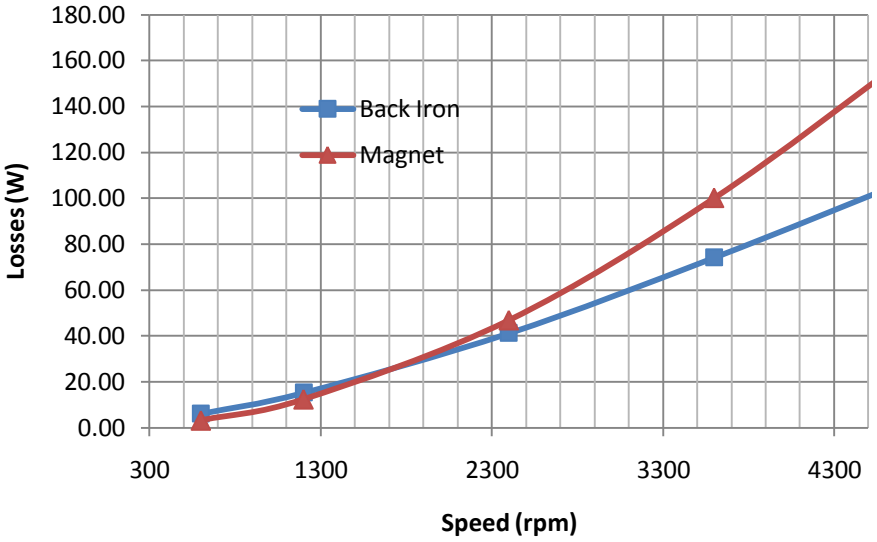

Figure 5.3 Variation of losses with speed at rated current for machine I using FEM

Table 5.1 Variation of losses with speed at current rated speed for Machine I

Eddy Current Losses	Rotor Speed (rpm)				
	600	**1200**	**2400**	**3600**	**4800**
Back Iron (W)	6.19	15.32	41.26	74.22	109.91
Magnet (W)	3.25	12.45	46.89	100.11	165.33

5.2.1.1 Variation of losses with stator current

In this simulation, the speed is kept constant at 3600 rpm while the current is varying from 30% to 120 % rated current.

Table 5.2 Variation of losses with current at rated speed for Machine I

Eddy Current Losses	% Rated Current (A)			
	30%	**75%**	**100%**	**120%**
Back Iron (W)	6.58	41.10	74.21	106.94
Magnet (W)	8.83	55.28	100.10	144.08

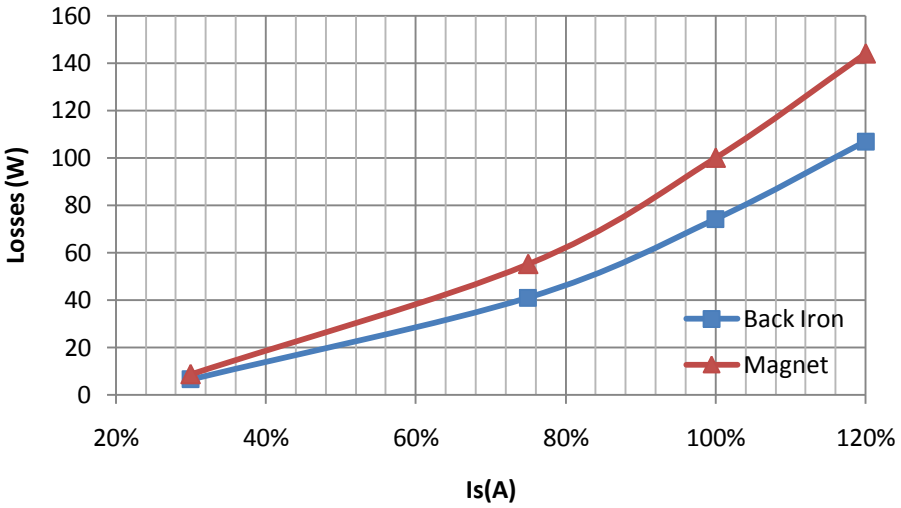

Figure 5.4 Variation of losses with current at rated speed for machine I using FEM

5.2.2 Machine II

Time consumed for this simulation was around 15-20 minutes for each current and speed conditions. For instantaneous time t = 2T, figure 5.5 (a) shows the flux density in the normal direction. In the sharp area, for example, in the corner of the tooth, the concentration of flux density is much higher than in the other area. Maximum value flux density could reach 5.9 T since in this simulation linear material properties are being used, in other words, there is no saturation effect.

Figure 5.5 (b) shows the distribution of the induced current (eddy current) while figure 5.5 (c) shows the distribution from the resistive heating (losses) in the back iron and magnet. Since it is assumed that the stator has zero conductivity, the eddy current losses only appear in the back iron and magnet. Induced current level for this condition can reach a maximum level 1.1×10^7 A/m^2, while surface resistive heating can reach value of $2{,}6 \times 10^7$ W/m^3 .

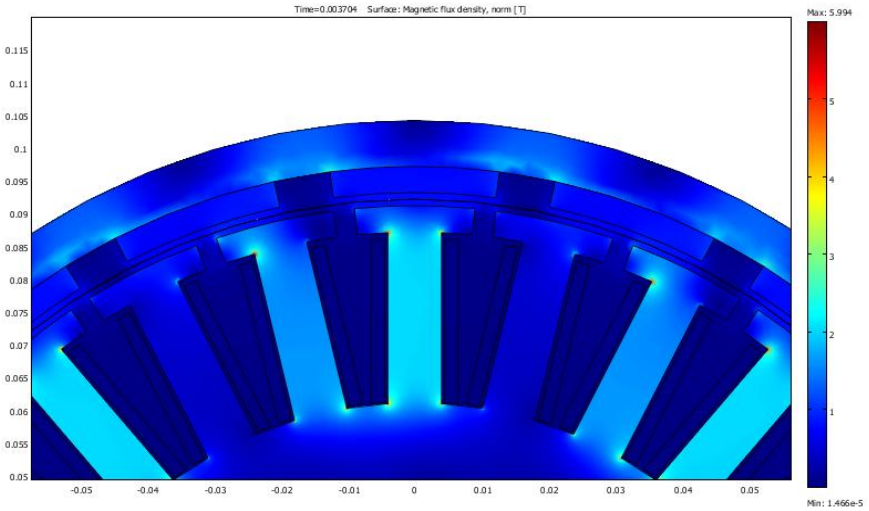

(a) normal flux density

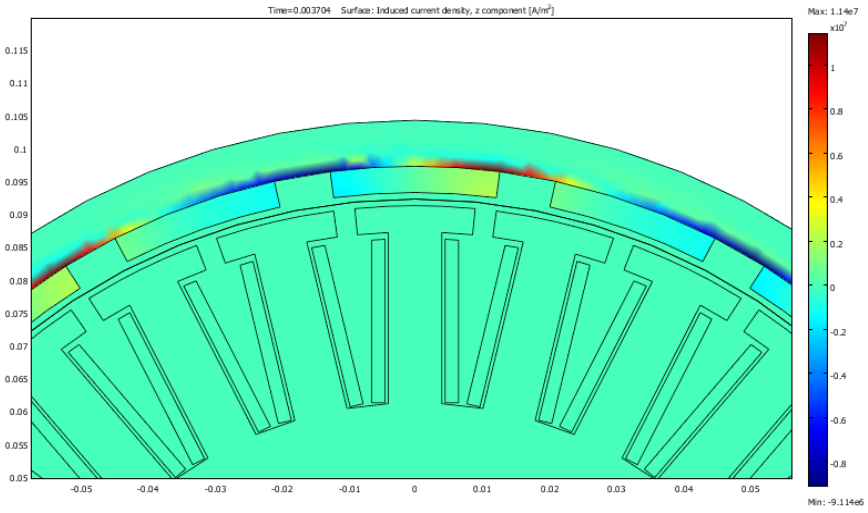

(b) Induced current density

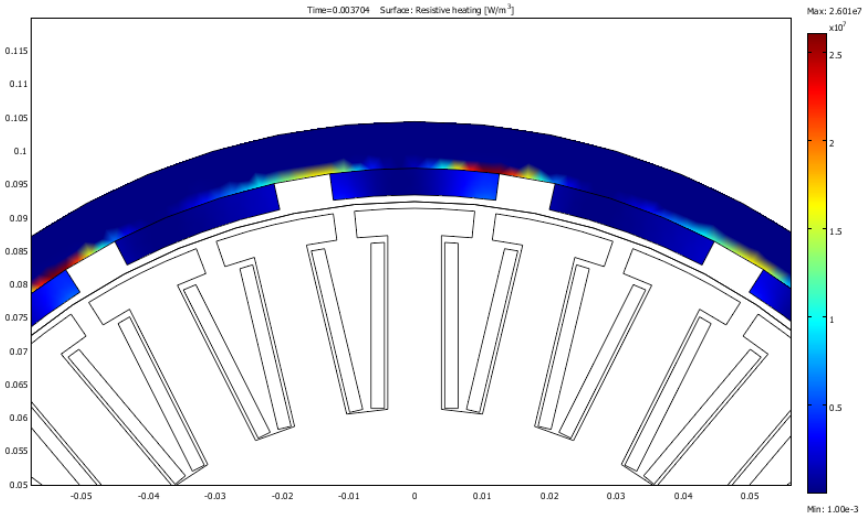

(c) resistive heating

Figure 5.5 Instantaneous condition machine II at t = 2T

5.2.2.1 Variation of losses with rotor speed

In this simulation, the stator current (Is) is kept at a constant value 5 A rms, while the speed vary from 600 to 4800 rpm. The losses for magnet and back iron are shown in figure 5.6 and table 5.3

Table 5.3 Variation of losses with speed at current rated speed for Machine II

Eddy Current Losses	Rotor Speed (rpm)				
	600	**1200**	**2400**	**3600**	**4800**
Back Iron (W)	8.54	23.04	60.58	106.34	158.56
Magnet (W)	4.97	18.93	70.20	148.19	247.85

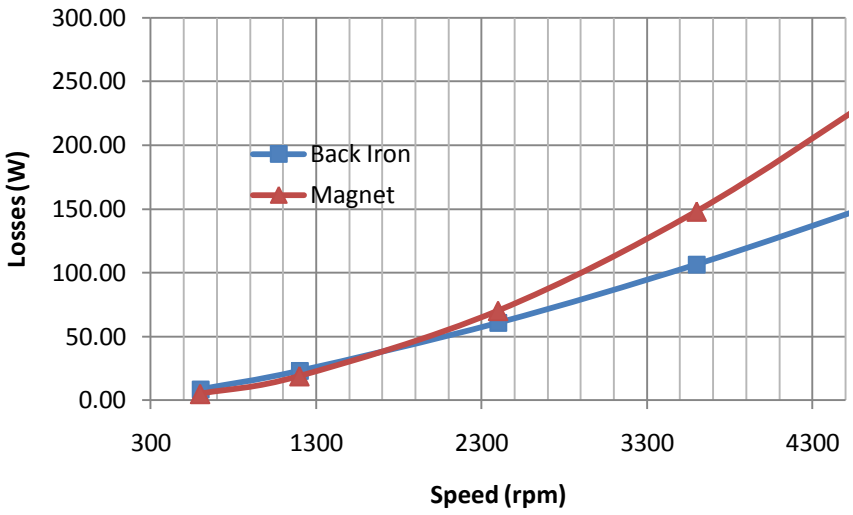

Figure 5.6 Figure 5.3 Variation of losses with speed at rated current for machine II using FEM

5.2.1.1 Variation of losses with stator current

In this simulation, the speed is kept at a constant rate of 3600 rpm, while the current is varied from 30% to 120 % rated current. Losses calculation results are shown in table 5.4 and figure 5.7.

Table 5.4 Variation of losses with current at rated speed for Machine II

Eddy Current Losses	% Rated Current (A)			
	30%	**75%**	**100%**	**120%**
Back Iron (W)	9.43	58.65	106.34	153.22
Magnet (W)	13.09	81.73	148.19	213.59

5.2.3 Machine III

Time consumed for this simulation around 15-20 minutes for each current and speed conditions. For instantaneous time t = 2T, figure 5.8 (a) shows the flux density in the normal direction. In the sharp area, for example, in the corner of the tooth, the concentration of flux density is much higher than in the other area. Maximum value flux density could reach 6.7 T since in this simulation linear material properties are being used, in other words, there is no saturation effect

Figure 5.8 (b) shows the distribution of the induced current (eddy current) while figure 5.8 (c) shows the distribution from the resistive heating (losses) in the back iron and magnet. Since it is assumed that the stator has zero conductivity, the eddy current losses only appear in the back iron and magnet. Induced current level for this condition can reach a maximum level 2.5×10^7 A/m^2, while surface resistive heating can reach value of $1,3 \times 10^8$ W/m^3.

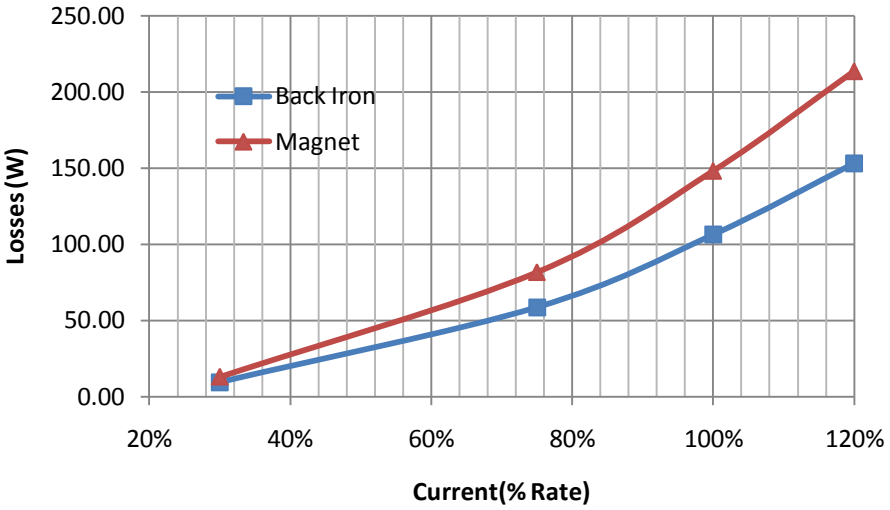

Figure 5.7 Variation of losses with current at rated speed for machine II using FEM

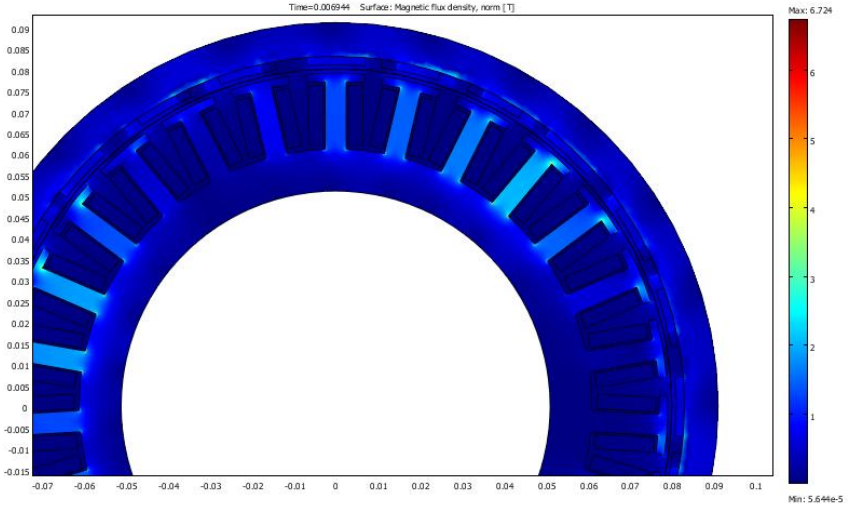

(a) normal flux density

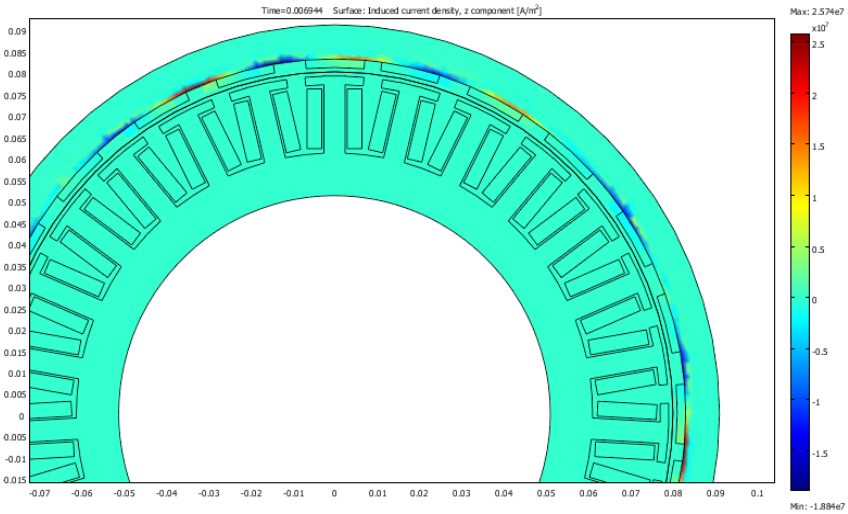

(b) Induced current density

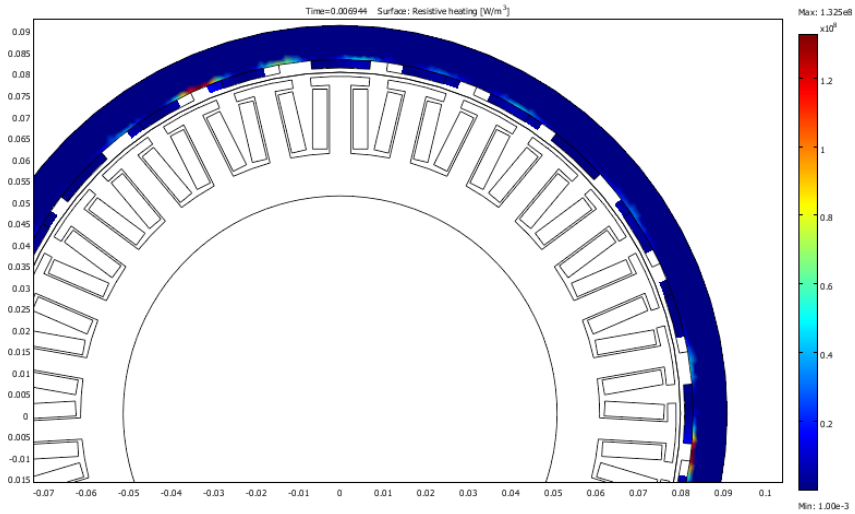

(c) resistive heating

Figure 5.8 Instantaneous condition machine III at t = 2T

Machine III has 9 tooth and 8 pole for each flux density wave length, winding configuration described in chapter IV, periodic condition for machine III is 8 pole, it figure 5.8 (b) and (c) the periodic of induced current and resistive heating for each 8 pole and 9 teeth, while the periodic condition for machine I and II is 2 pole and 3 tooth showed by figure 5.2 and 5.5.

5.2.3.1 Variation of losses with rotor speed

In this simulation, stator current (Is) is kept at constant value of 2.1 A rms, while the speed is varied from 600 to 4800 rpm. The losses for magnet and back iron are shows in figure 5.9 and table 5.5.

Table 5.5 Variation losses with speed at current rated speed for Machine III using FEM

Eddy Current Losses	Rotor Speed (rpm)				
	600	**1200**	**2400**	**3600**	**4800**
Back Iron (W)	18.23	46.42	116.20	197.93	301.44
Magnet (W)	4.42	15.93	56.35	117.23	199.88

5.2.1.1 Variation of losses with stator current

In this simulation, the speed is kept constant at a value of 3600 rpm while the current is varied from 30% to 120 % rated current. Losses calculation results are shown in table 5.6 and figure 5.10.

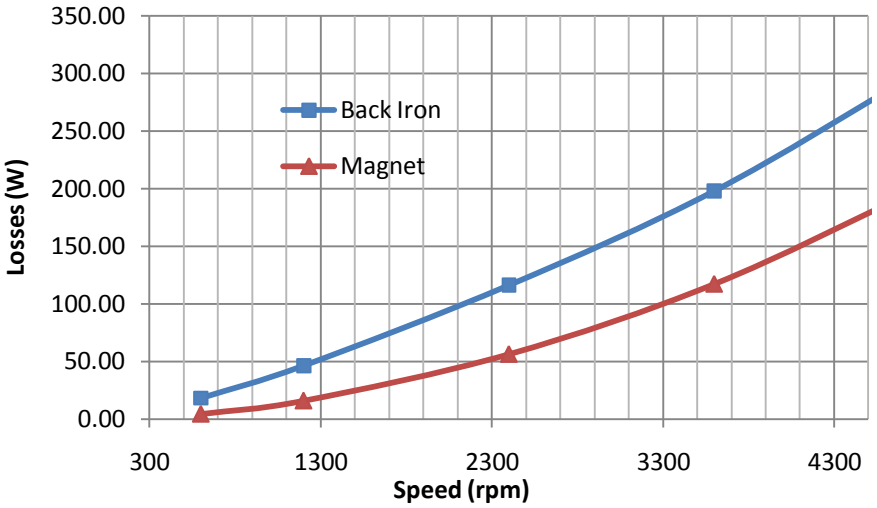

Figure 5.9 Variation losses with speed at rated current for machine III using FEM

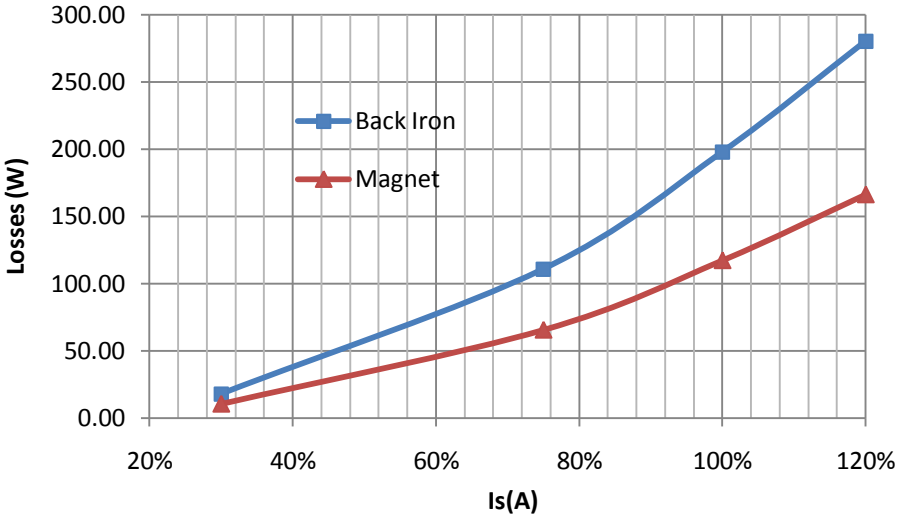

Figure 5.10 Variation losses with current at rated speed for machine III using FEM

Table 5.6 Variation losses with current at rated speed for Machine II using FEM

Eddy Current Losses	% Rated Current (A)			
	30%	**75%**	**100%**	**120%**
Back Iron (W)	17.85	110.76	197.93	280.32
Magnet (W)	10.56	65.57	117.23	166.18

5.2.4 Slotting Effect

For this simulation, the slotting effect is investigated. There is no load losses condition, this condition when the rotor is running at a rated speed of 3600 rpm at generator mode with zero current in the stator. To obtain more data about slotting effect, two dummy machines with different length of slot opening are added.

Figure 5.11 show the difference of air gap flux distribution for slot opening having four different length of slot opening. It shows the influence of slotting the distribution of air gap flux density. In the opening slot area shown that the change of flux density is being influenced by the length of slot opening.

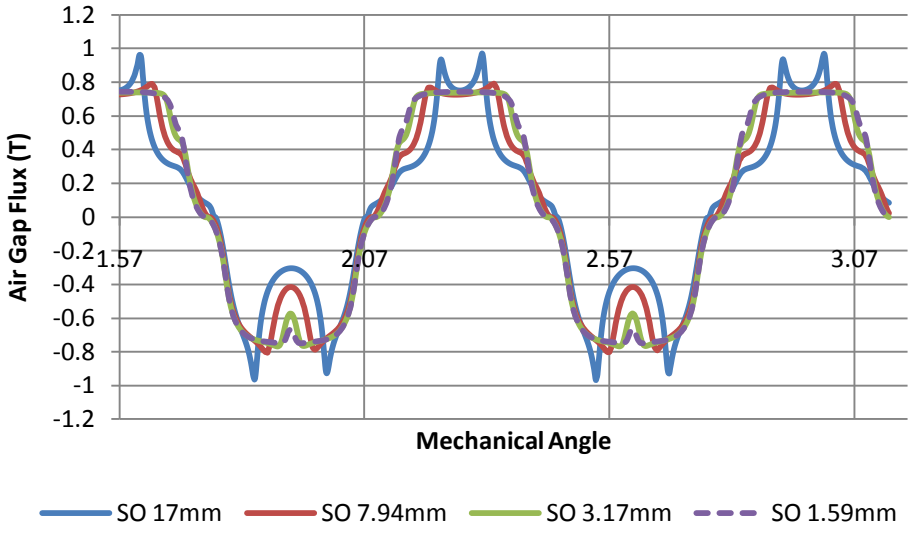

Figure 5.11 Slotting effect to air gap flux density

The change of the air gap flux density in no-load condition, is only being influenced by the difference of permeance between the slot and the tooth, and by the induce current at magnet and back iron produced by the change of the flux density. Once the induced current appear in material with non zero conductivity, the eddy current losses will appear.

Figure 5.12 shows the variation of no-load losses due to the change of slot opening. It shows that the losses in back iron and magnet would increase rapidly for longer slot opening.

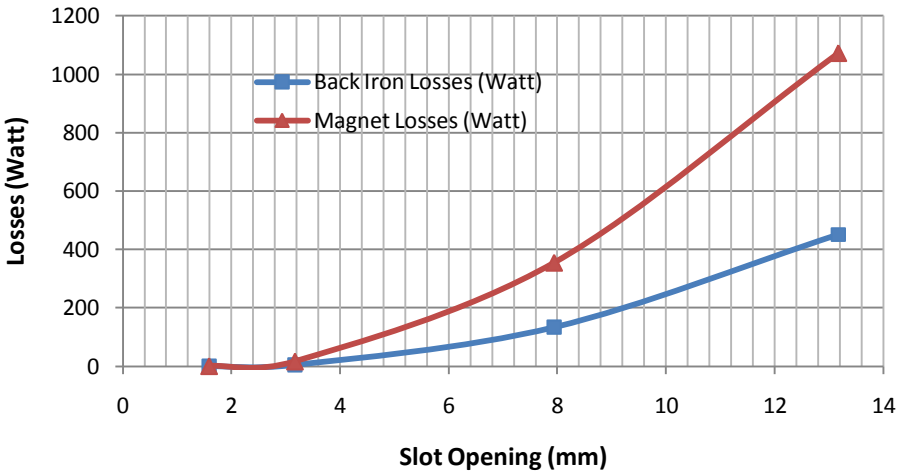

Figure 5.12 Variation of no load losses with slot opening

Figure 5.13 shows the distributions of losses for a slot opening of 3.17 mm. Losses concentration is located in the slot opening area. The reason is quite clear since the change of flux

density in this area is much higher, as it was shown in figure 5.12 the location of slot opening having rapid change in flux density.

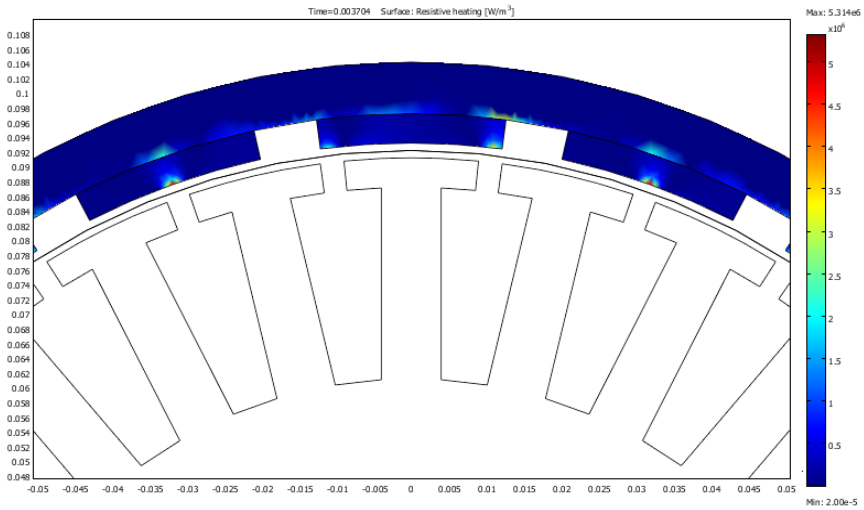

Figure 5.13 Losses distribution for slot opening 3.17 mm.

5.2.5 Non Linear Effect

In this simulation, the property of the stator material is changed from linear material to soft iron material silicon steel. The magnetic material properties are shown in figure 5.14.

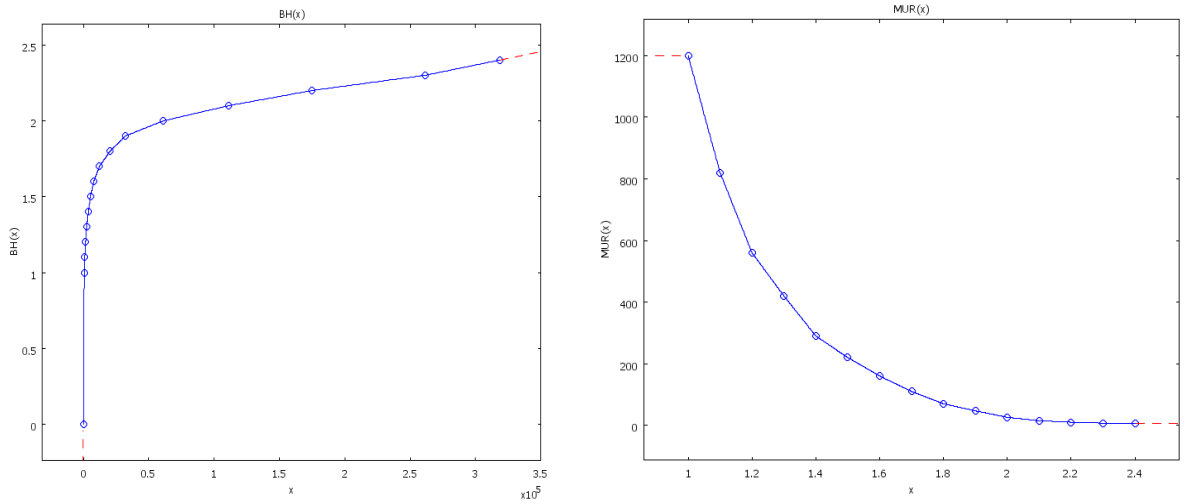

(a) (b)

Figure 5.14 Silicon steel material properties (a) B-H curve (b) μ_r –B Curve

Since the constitutive relation between B and H is not linear, in the simulation we change the constitutive relation on stator to form equation 2.7 to equation 2.32. The result for Machine II running at 3600 rpm while having stator current 5 A is shown in figure 5.15.

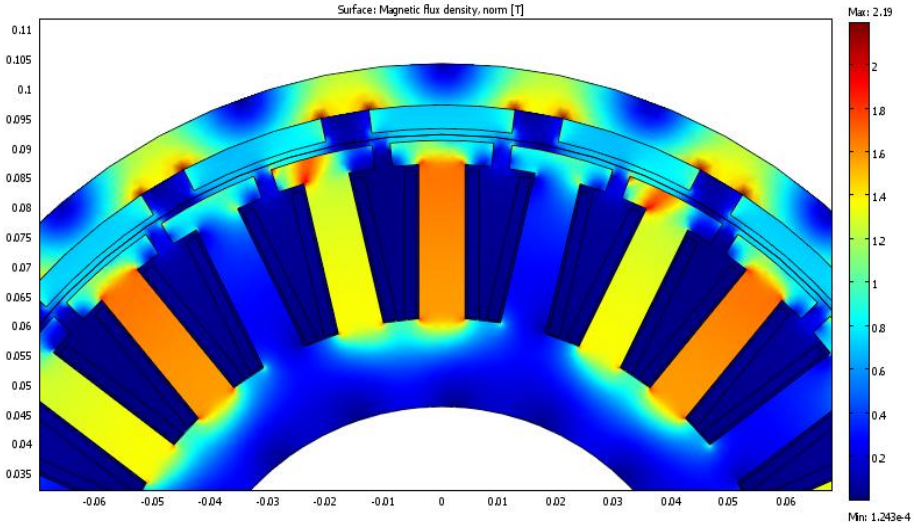

(a) Flux density

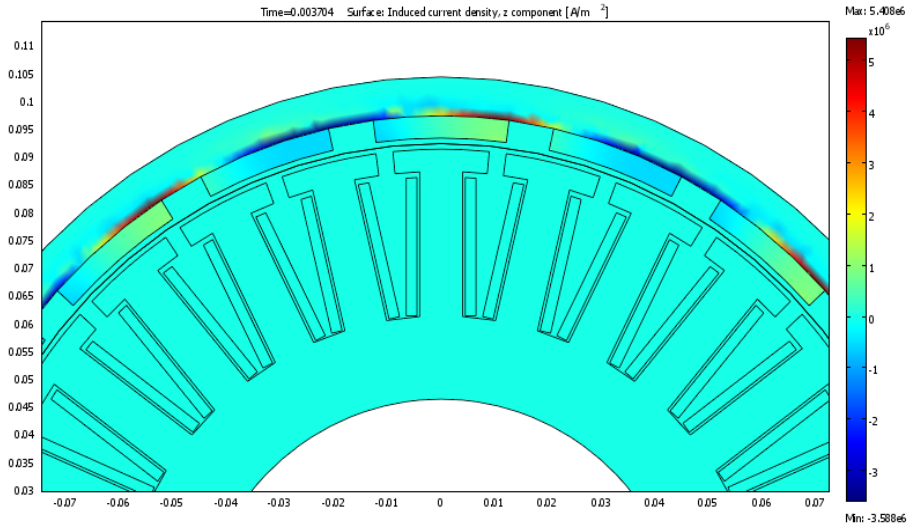

(b) Induced current density

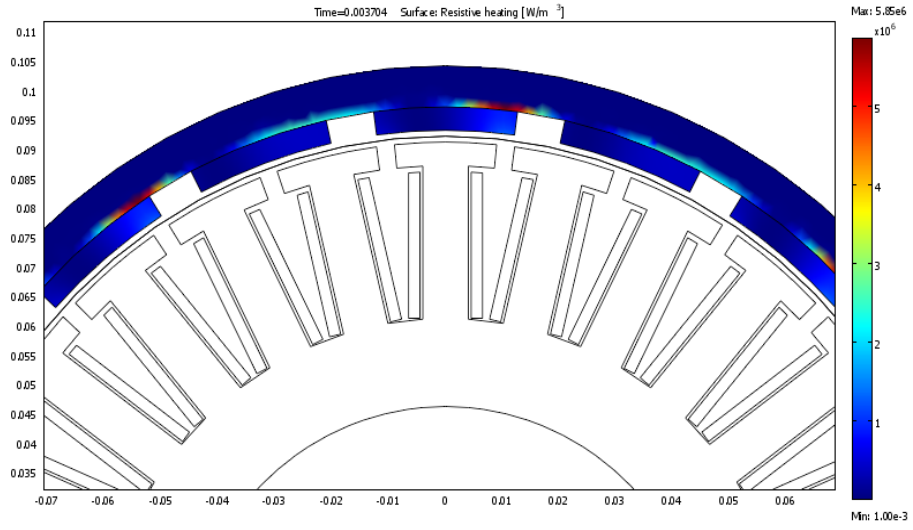

(c) resistive heating

Figure 5.15 Instantaneous condition machine II at t = 2T with soft magnetic material in stator

Time consumed for this simulation around 30-40 minutes using default setting from COMSOL, by analytical calculation of μ_r [see chapter 2.6.3] computational time reduces to 15-20 minutes.

Figure 5.15 (a) shows the distribution of the flux density. The maximum flux density is 2.19 T. This value decreases from 5.9 T in the linear stator model shown in figure 5.5a. The maximum surface-induced current decrease from $1.1x10^7$ A/m^2 to $5.4x10^6$ A/m^2 .Maximum surface resistive heating also decrease from 2.6×10^7 W/m^3 to 5.8×10^6 W/m^3.

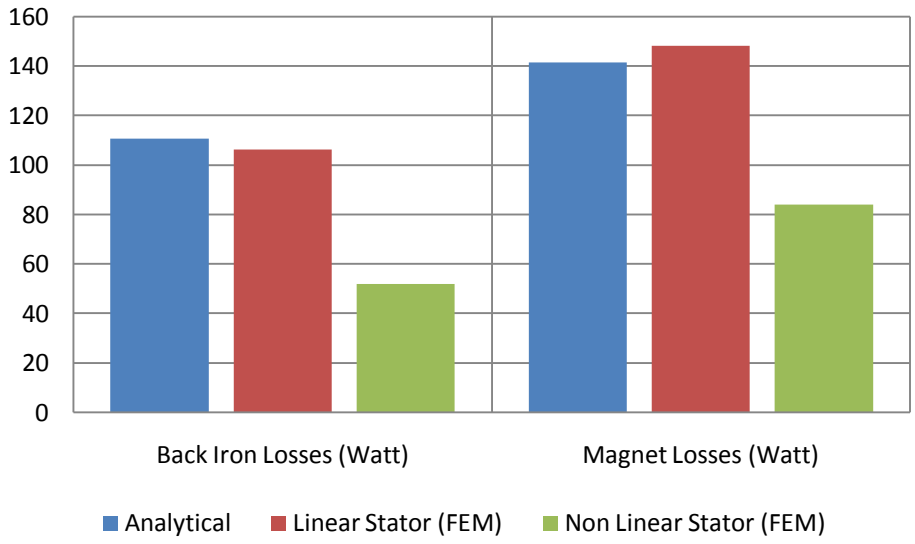

Figure 5.16 Effect non-linear Material to no load losses

Figure 5.16 shows the losses comparison between analytical calculation, FEM result of the linear stator material and FEM result of the non linear stator material at the rated current and speed of machine II. This result shows that the losses of non linear material are much lower than analytical calculation and linear stator material.

Chapter 6

RESULT AND DISCUSSION

6.1 Back iron losses comparison

The eddy current losses calculation results in back iron using both analytical and finite element are summarized in table 6.1 and 6.2. The analytical result shows quite good approximation. For speed higher than 2400 rpm, the deviation between analytical and FEM is around 5% For speed higher than the rated speed analytical calculation shows lower than the FEM result while in low speed condition the analytical calculation result higher than FEM result.

Table 6.1 Variation of back iron losses with speed at rated current

Back Iron Losses	Rotor Speed (Rpm)				
	600	1200	2400	3600	4800
Machine I Analytical (Watt)	5.33	14.94	40.91	74.14	114.27
Machine I FEM (Watt)	5.63	15.32	41.26	74.22	109.91
Deviation (%)	**5.30**	**2.48**	**0.85**	**0.11**	**-3.97**
Machine II Analytical (Watt)	7.30	21.08	60.03	110.53	167.36
Machine II FEM (Watt)	8.54	23.04	60.58	106.34	158.56
Deviation (%)	**14.56**	**8.49**	**0.91**	**-3.94**	**-5.55**
Machine III Analytical (Watt)	16.78	43.67	109.94	201.68	303.72
Machine III FEM (Watt)	18.23	46.42	116.20	197.93	301.44
Deviation (%)	**7.95**	**5.93**	**5.39**	**-1.89**	**-0.76**

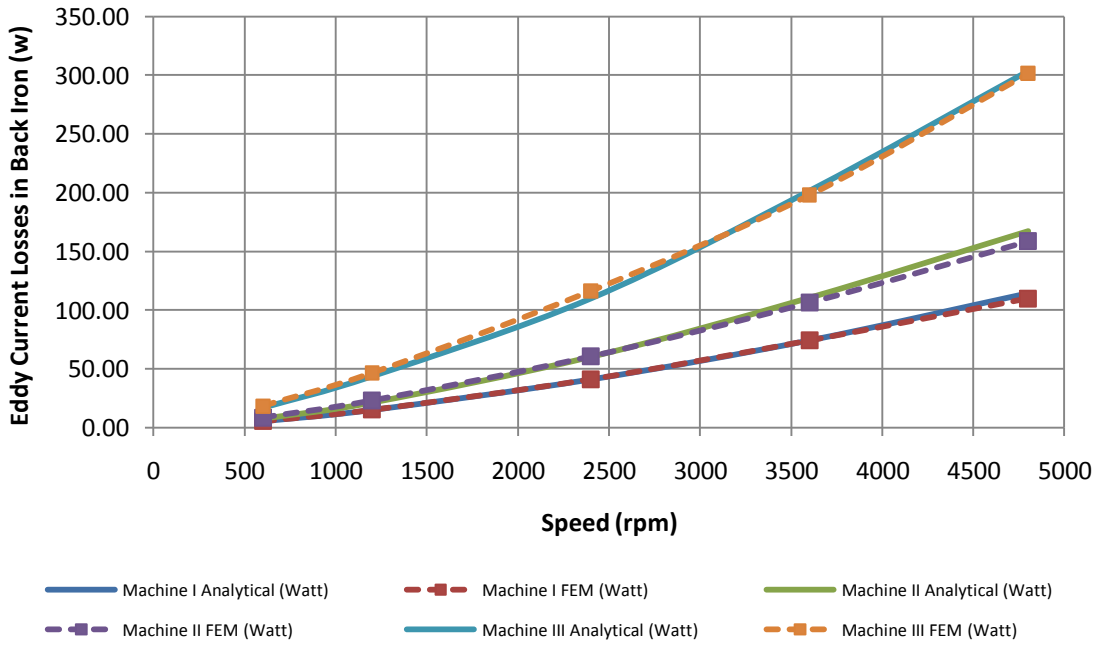

Figure 6.1 Variation of back iron loss with rotor speed at rated current using Analytical and FEM

Table 6.2 shows the comparison between results obtained from analytical and FEM, the comparison show quite close having deviation around 5% in all range of current. From these comparison results, it can be conclude analytical model for the calculation of the eddy current losses in the back iron is quite accurate.

Table 6.2 Variation of back iron losses with stator current at rated speed

Back Iron Losses	% Stator rated current			
	30%	75%	100%	120%
Machine I Analytical (Watt)	6.67	41.7	74.14	106.77
Machine I FEM (Watt)	6.58	41.10	74.22	106.94
Deviation (%)	**-1.30**	**-1.46**	**0.11**	**0.16**
Machine II Analytical (Watt)	9.95	62.17	110.53	159.72
Machine II FEM (Watt)	9.43	58.65	106.34	153.22
Deviation (%)	**-5.52**	**-6.00**	**-3.94**	**-4.25**
Machine III Analytical (Watt)	18.15	113.45	201.68	290.42
Machine III FEM (Watt)	17.85	110.76	197.93	280.32
Deviation (%)	**-1.69**	**-2.43**	**-1.89**	**-3.60**

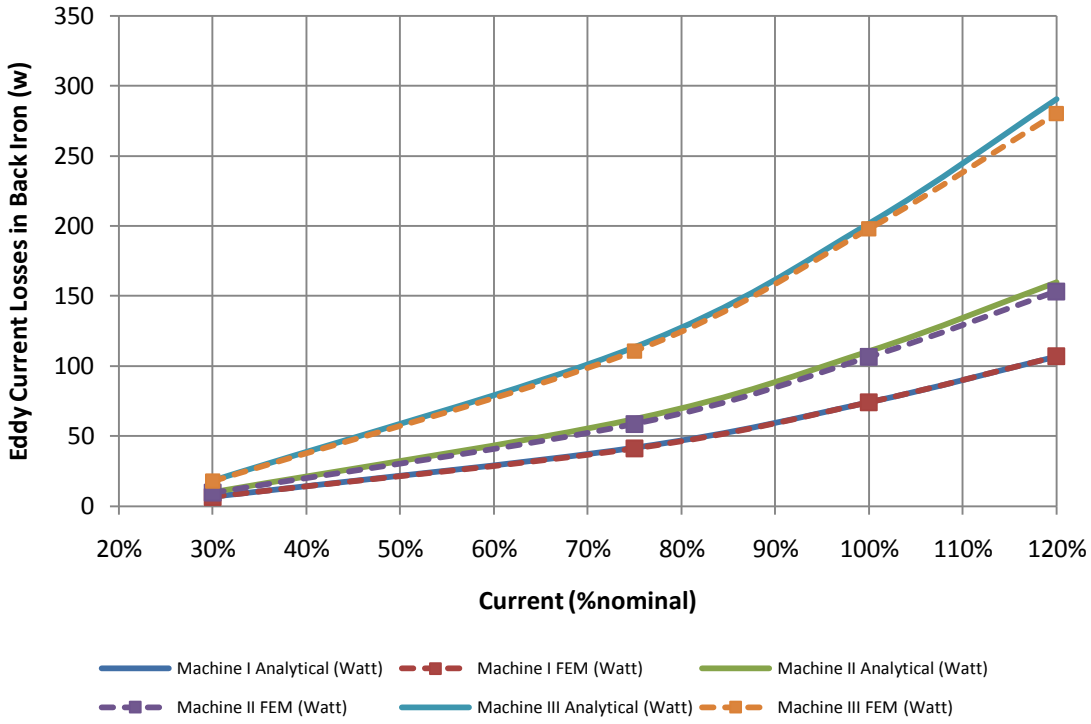

Figure 6.2 Variation of back iron loss with stator current at rated speed using Analytical and FEM

6.2 Magnet losses comparison

Table 6.3 shows the comparison result for magnet losses between analytical methods described in chapter 4.3. For low speed, the deviation between the two result quite big. At 600 rpm

speed, the deviation is more than 20%, but at higher speed, the deviation between analytical and FEM is less than 10%. The FEM result is nearly positive in all range of speed.

Table 6.3 Variation of magnet losses with speed at rated current

Magnet Losses	Rotor Speed (Rpm)				
	600	1200	2400	3600	4800
Machine I Analytical (Watt)	2.56	10.25	41.00	92.27	164.04
Machine I FEM (Watt)	3.25	12.45	46.89	100.11	165.33
Deviation (%)	**21.12**	**17.66**	**12.56**	**7.83**	**0.78**
Machine II Analytical (Watt)	3.93	15.72	62.87	141.45	251.46
Machine II FEM (Watt)	4.97	18.93	70.20	148.19	247.85
Deviation (%)	**21.00**	**16.94**	**10.44**	**4.55**	**-1.46**
Machine III Analytical (Watt)	2.94	11.78	47.10	105.98	188.41
Machine III FEM (Watt)	4.42	15.93	56.35	117.23	199.88
Deviation (%)	**33.45**	**26.07**	**16.41**	**9.60**	**5.74**

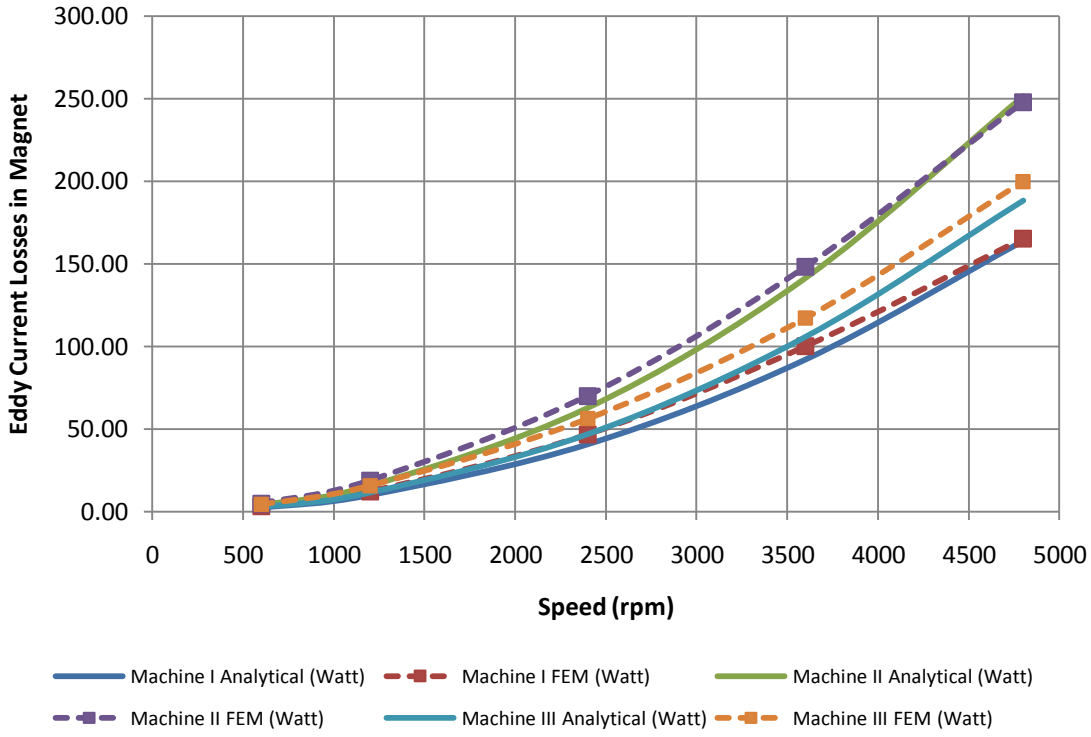

Figure 6.3 Variation of magnet losses with rotor speed at rated current using Analytical and FEM

Table 6.4 and figure 6.4 shows the deviation between Analytical and FEM results independent to the stator current, it is shown that the speed variation has a big influence in determining the deviation result.

Table 6.4 Variation of magnet losses with stator current at rated speed

Magnet Losses	% Stator rated current			
	30%	75%	100%	120%
Machine I Analytical (Watt)	8.30	51.90	92.27	132.87
Machine I FEM (Watt)	8.83	55.29	100.11	144.09
Deviation (%)	**6.04**	**6.13**	**7.83**	**7.79**
Machine II Analytical (Watt)	12.73	79.56	141.45	203.68
Machine II FEM (Watt)	13.09	81.73	148.19	213.59
Deviation (%)	**2.78**	**2.66**	**4.55**	**4.64**
Machine III Analytical (Watt)	9.54	59.61	105.98	152.61
Machine III FEM (Watt)	10.56	65.57	117.23	166.18
Deviation (%)	**9.67**	**9.08**	**9.60**	**8.16**

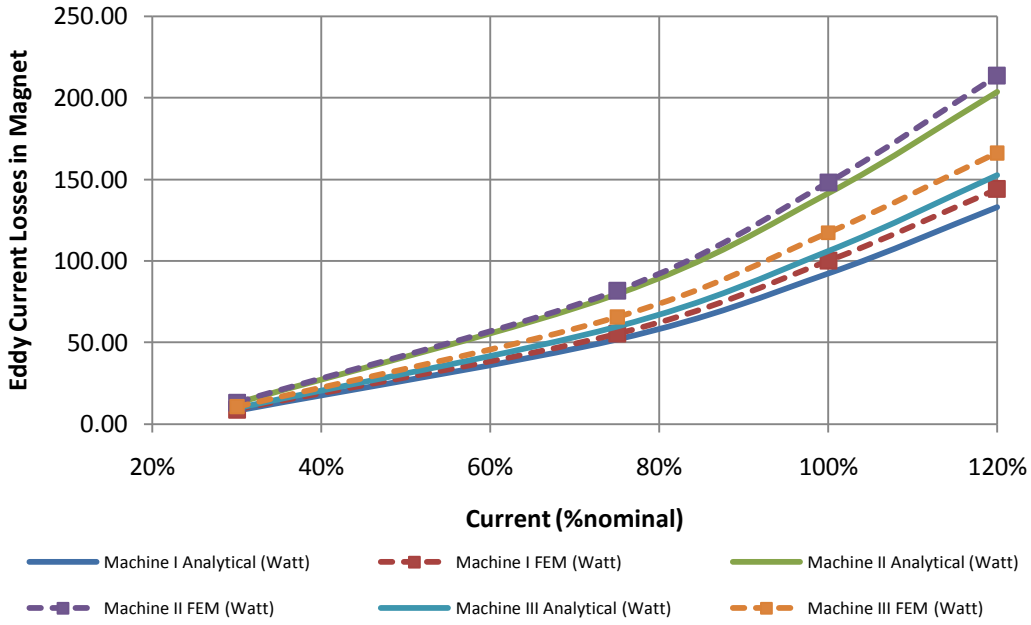

Figure 6.4 Variation of magnet losses with stator current at rated speed using Analytical and FEM

6.3 Slotting Effect

Table 6.5 shows the effect of slot opening to no-load losses. The losses in back iron increases from 0.31 watt for slot opening of 1.59 mm to 450.83 watt for slot opening of 13.17 mm. Magnet losses increases from 1.2 watt to 1071.72 watt when slot opening is change from 1.59 mm to 13.17 mm.

Table 6.5 Variation of no load losses with slot opening

Slot Opening (mm)	1.59	3.17	7.94	13.17
Magnet losses (watt)	1.2	17.03	133.70	1071.72
Back iron losses (watt)	0.31	5.05	354.78	450.83

Since the magnitude of the eddy current losses is influenced by the change of flux density, and machines with longer slot opening have bigger eddy current losses, for the same rotor speed, a machine with longer slot opening will have higher flux density change. Figure 5.11 explains the slot opening effect to air gap flux density.

6.4 Material non-linearity effect

Table 6.6 shows the comparison of losses in back iron and magnet by applying non linear material in stator. This simulation is for machine II running at a speed of 3600 rpm and having a stator current of 5 A rms, It is show that the losses in back iron and magnet decreases if non-linear material such as soft magnetic material in this simulation is used in the rotor.

Table 6.6 Effect non-linear Material to no load losses

	Back Iron Losses (Watt)	Magnet Losses (Watt)
Analytical	110.53	141.45
Linear Stator (FEM)	106.34	148.19
Non Linear Stator (FEM)	51.87	83.92

Non linear stator material limits the maximum of flux density in the saturation area, As a result, the maximum flux density decreases from 5.9 T in the linear stator model to 2.19 T in non linear stator model, It can be seen from the B-H curve of cast iron in figure 5.14 (a) and (b), saturation region of this material in area of B is higher than 1.5 T. The reduced amplitude of the flux density influences the change of the flux density. Then the eddy current losses also decrease as the consequence of the decrease of flux density change.

Non linear effect is not taken into account in the analytical prediction. As a result there is a big deviation between analytical and non linear FEM results.

Chapter 7

CONCLUSSION AND FUTURE WORK

7.1 Contributions and Conclusions

This project deals with the calculation of eddy current losses in back iron and magnet for concentrated permanent magnet machine. Eddy current losses of the three machines models from Mastervolt Company (described in chapter IV) is calculated using both analytical and finite element methods (FEM). Here are two major issues to be compared between these two methods:

1. Computation time

- Computation time using finite element methods take long time from preparation until simulation. Average time for one simulation with linear material is around 15-20 minutes whereas for non-linear material the computation time is increased to be 30-40 minutes. Improving the methods to calculate the permeability using analytical solution in non linear material [18] can decrease computation time in half (15-20 minutes).
- Since analytical method gives result in the fastest way, it is easy to change the parameter of the models and, thus, suitable for the initial process of generator design.

2. Calculation results

- Deviated results between analytical and FEM for back iron losses calculation are varying from 14.57 % to -5.55% and the speed varies between 600 rpm and 4800 rpm. At low speed the deviation trend is positive while in the high speed it tends to be negative.
- Deviated results between analytical and FEM for back iron losses calculation tend to be constant around -5% at rated speed although the current is varied between 30% to 120% of rated current.
- Deviated results between analytical and FEM for magnet losses calculation vary from 33.45 % to -1.46% and the speed varies between 600 rpm to 4800 rpm. At low speed the deviation trend is positive while in the high speed it tends to be negative.
- Deviation results between analytical and FEM for back iron losses calculation are tend to be constant around 10 % at rated speed although the current is varied between 30% and 120% of rated current.
- Finite element method can be used to calculate no load eddy current losses whereas analytical method cannot be.

- When applied to non linear material in stator, a big difference in the calculation result is found using and analytical method (around 40%). However, since in the real condition stator material always has non linear characteristic, finite element method will give more accurate result then analytical method.
- Finite element method can also be used to calculate geometry effect, for example slot opening distance, to the eddy current losses which is not properly accommodated in analytical method.
- Both distribution (location) and magnitude of eddy current losses can also be presented in the result of finite element simulation.

7.2 Future work

1. Analytical method is very useful in the initial stage of generator design. For better accuracy result, analytical method should be improved to accommodate non-linear material and other geometry effects.
2. To accommodate end effects and to obtain better accuracy in finite element model, it is suggested to use 3D model in the simulation.
3. Validation of the eddy current losses calculation with the laboratory measurement.

REFFERENCES

[1] http://ec.europa.eu/energy/energy_policy/doc/01_energy_policy_for_europe_en.pdf

[2] http://www.ewea.org/fileadmin/ewea_documents/documents/statistics/energy_mix.pdf

[3] H.Polinder, S.W.H. De haan, Maxime.R.Dubois,J.G.Slotweg, "Basic Operation Principles and Electrical Conversion Systems of Wind Turbines", *Nordic Workshop on Power and Industrial Electronics*, Paper ref 069, Trondheim, 14-16 June, 2004.

[4] Koch.T, Binder.A, Machines, "Permanent magnet machines with fractional slot winding for electric traction", *Proc. International Conference on Electrical Machines*, Brugge, Belgium, August 25-28, 2002.

[5] F.Magnussen, P.Thelin,C.Sadarangani, "Analysis of a PM Machine with Concentrated Fractional Pitch Windings", *Nordic Workshop on Power and Industrial Electronics*, Paper ref 069, Trondheim, 14-16 June, 2004.

[6] K.J.Binns, P.J. Lawrenson,C.W Trowbridge, *The Analytical and Numerical Solution of Electric and Magnetic Fields*, John Wiley and Sons, 1992.

[7] A.B.J Reece,T.W. Preston, *Finite Element Methods in Electrical Power Engineering,* Oxford University Press, 2000.

[8] Nicola Bianchi, *Electrical Machine Analysis Using Finite Elements*, CRC Press, 2005.

[9] A.Bondeson, T.Rylander, Pa¨r Ingelstro¨m, *Computational Electromagnetic*, Springer, 2005.

[10] Fred Vermolen, Domenico Lahaye, *"Introduction to Finite Elements"*, Lecture Notes, TU Delft, 2008.

[11] J.Donea, Antonio Huerta, J.-Ph. Ponthot, A.Rodr´ıguez-Ferran, *"Arbitrary Lagrangian Eulerian methods"*, Encyclopedia of computational mechanics, Vol.1 Chapter 14, John Wiley and Sons, 2004.

[12] H.Polinder, M.J. Hoijmakers, M.Scuotto, "Eddy-current losses in solid back iron of permanent magnet machines with concentrated fractional pitch winding", *IEEE International Conference on Power Electronic, Machines and Drives*, Dublin, 4-6 April 2006, pp.333-339, vol.1.

[13] H.Polinder, M.J. Hoijmakers, M.Scuotto,, "Eddy-current losses in solid back iron of permanent magnet machines for different concentrated fraction pitch winding", *IEEE International Electric Machine and Drives Conference 2007*, Volume 1, 3-5 May 2007, pp. 652-657.

[14] Kais Atallah, "Rotor loss in permanent-magnet brushless ac machine", *IEEE Transaction on industry application*, Vol.36, pp 1612-1618, Nov 2000.

[15] D.Ishak, Z.Q Zhu, David Howe, "Eddy-current loss in the rotor magnets of permanent-magnet brushless machines having fractional number slots per pole", *IEEE Transactions on magnetic*, Vol.41, pp 2462-2469, Sept 2005.

[16] Comsol Multiphysics Reference Guide, Comsol AB, 2007.

[17] Comsol Multiphysics AC/DC Module User Guide, Comsol AB, 2007.

[18] Domenico Lahaye, “Winded Coils and Ferromagnetic Cores in Comsol Multiphysics”, Inventory Notes, Delft Univ. Tech , Delft, The Netherland 2009.

[19] A.K Jassal, “Design of 2.25 MW, PM ,Direct Drive Generator for Wind Energy Applications Using Concentrated Windings and Minimizing Eddy Current Losses in the Rotor Back Iron”. MSc Thesis, Delft Univ. Tech , Delft, The Netherland 2008.

[20] H.Polinder, “On the losses in a high-speed permanent magnet generator with rectifier”, Ph.D. Dissertation, Delft Univ. Tech, The Netherland, 1998.

[21] Robert Holm, “Modelling and optimazion of a permanent magnet machine in a flywheel, Ph.D. Dissertation, Delft Univ. Tech, The Netherland, 2003.

[22] P.J. Lawrenson, P.Reece, M.C. Ralph, “Toth-ripple losses in solid poled”, Proceeding of the IEE, vol.113, pp. 657-662 (1996).

[23] Juha Pyrh¨onen, Tapani Jokinen, Val´eria Hrabovcov´, *Design of rotating electrical machines*, John Wiley and Sons, 2008.

APPENDIX

The no load air gap flux density

$$B_g = \frac{l_m}{\mu_{rm} g_{eff}} B_r$$

Fundamental component of air gap flux

$$B_{g1} = \frac{l_m}{\mu_{rm} g_{eff}} B_r \frac{4}{\pi} \sin(\frac{b_p}{\tau_p} \frac{\pi}{2})$$

Effective air gap leght

$$g_{eff} = k_c (g + \frac{l_m}{\mu_{rm}}) \text{ and}$$

$$\gamma = \frac{4}{\pi} \left(\frac{b_{so}}{2\left(g + \frac{l_m}{\mu_{rm}} \right)} * \tan^{-1} \frac{b_{so}}{2\left(g + \frac{l_m}{\mu_{rm}} \right)} - \ln \sqrt{1 + \left(\frac{b_{so}}{2\left(g + \frac{l_m}{\mu_{rm}} \right)} \right)^2} \right)$$

Carter factor

$$k_c = \frac{\tau_s}{\tau_s - \gamma \left(g + \frac{l_m}{\mu_{rm}} \right)}$$